

NASA/TP—1998—208608



Elementary Theoretical Forms for the Spatial Power Spectrum of Earth's Crustal Magnetic Field

C. Voorhies, Goddard Space Flight Center, Greenbelt, Maryland

National Aeronautics and
Space Administration

Goddard Space Flight Center
Greenbelt, Maryland 20771

December 1998

Acknowledgments

Joy A. Conrad accurately and efficiently coded and quickly ran most of the computations summarized in this paper and prepared the Figures. She deserves, but declines, coauthorship (having long since moved to Houston to do more critical programming for the Shuttle). My special thanks to A. Jackson and the late M. McLeod for drawing attention to a fundamental and interesting geophysics problem, to J. Cain and M. Purucker for sharing the results of their analyses, and to T. Ravat for encouraging discussions. My thanks to the people of the United States of America who supported this work through their National Aeronautics and Space Administration, research and technological operating plans 579-31-07, 579-31-08, and 670-72-03.

Available from:

NASA Center for AeroSpace Information
Parkway Center/7121 Standard Drive
Hanover, Maryland 21076-1320
Price Code: A17

National Technical Information Service
5285 Port Royal Road
Springfield, VA 22161
Price Code: A10

ABSTRACT

The magnetic field produced by magnetization in Earth's crust and lithosphere can be distinguished from the field produced by electric currents in Earth's core because the spatial magnetic power spectrum of the crustal field differs from that of the core field. Theoretical forms for the spectrum of the crustal field are herein derived by treating each magnetic domain in the crust as the point source of a dipole field. The geologic null-hypothesis that such moments are uncorrelated is used to obtain the magnetic spectrum expected from a randomly magnetized, or unstructured, spherical crust of negligible thickness. This simplest spectral form is modified to allow for uniform crustal thickness, ellipsoidality, and the polarization of domains by an aperiodically reversing, geocentric axial dipole field from Earth's core. Such spectra are intended to describe the background crustal field. Magnetic anomalies due to correlated magnetization within coherent geologic structures may well be superimposed upon this background; yet representing each such anomaly with a single point dipole may lead to similar spectral forms. Results from attempts to fit these forms to observational spectra, determined via spherical harmonic analysis of MAGSAT data, are summarized in terms of amplitude, source depth, and misfit.

Each theoretical spectrum reduces to a source factor multiplied by the usual exponential function of spherical harmonic degree n due to geometric attenuation with altitude above the source layer. The source factors always vary with n and are approximately proportional to n^3 for degrees 12 through 120. The theoretical spectra are therefore not directly proportional to an exponential function of spherical harmonic degree n . There is no radius at which these spectra are flat, level, or otherwise independent of n .



1. Introduction

In the enduring absence of magnetic monopoles, magnetic induction is a solenoidal vector field caused by electric currents. Macroscopic magnetic induction, or magnetic flux density, \mathbf{B} is often partitioned into the magnetic field strength \mathbf{H} due to conduction currents and magnetization \mathbf{M} due to magnetization currents

$$\mathbf{B} = \mu_0(\mathbf{H} + \mathbf{M}), \quad (1a)$$

where μ_0 represents the scalar vacuum magnetic permeability. This partitioning reflects the difference between the extrinsic linear velocity and the intrinsic angular velocity of an elementary electrically charged particle. Macroscopic net drift of many such charges gives a conduction current; macroscopic net spin of charges gives a magnetization current.

Here attention is focused upon the slowly varying, quasi-steady magnetic field due to natural sources within and near planet Earth. The main source of Earth's main magnetic field is evidently electric current flowing in Earth's roughly spherical, electrically conducting, ferro-metallic liquid outer core and solid inner core. Other sources of the geomagnetic field include weaker currents in the electrically resistive, ferro-magnesian silicate and oxide mantle; magnetization in the colder lithosphere and crust; and electric currents in the saline hydrosphere, the ionosphere above, and the magnetosphere beyond. In the pervasive presence of sources, the geomagnetic field can be represented in terms of poloidal and toroidal vector fields and associated scalars (see, e.g., Backus [1986]); however, the potential field representation remains appropriate for those portions of the total field with sources located outside the region of observation.

1.1 The Geomagnetic Field of Internal Origin

In an effectively source-free region, the geomagnetic induction \mathbf{B}_g is treated as a purely poloidal, scaloidal, potential field given by the negative gradient of a scalar potential V_g that satisfies Laplace's equation. This field is mathematically separable into the internal source field \mathbf{B}_{int} and the external source field \mathbf{B}_{ext} according to the location of the sources relative to a reference surface

$$\begin{aligned} \mathbf{B}_g &= -\nabla V_g \\ &= -\nabla(V_{int} + V_{ext}) = \mathbf{B}_{int} + \mathbf{B}_{ext}. \end{aligned} \quad (1b)$$

If the reference surface is the roughly ellipsoidal base of Earth's atmosphere, then equation (1b) omits non-potential fields from electric currents in the lowest atmosphere (e.g., cloud-to-ground lightning).

To focus attention upon "the core field" \mathbf{B}_c and "the crustal field" \mathbf{B}_x , both externally induced internal fields \mathbf{B}_{ind} (attributed to conduction currents induced within the Earth by time-varying external source magnetic fields) and hydrospheric fields \mathbf{B}_h (due to conduction currents in the oceans) are omitted

$$\begin{aligned} \mathbf{B}_{int} &= -\nabla V_{int} = \mathbf{B}_c + \mathbf{B}_x + (\mathbf{B}_{ind} + \mathbf{B}_h) \\ &= \mathbf{B}_c + \mathbf{B}_x. \end{aligned} \quad (1c)$$

The core field is mainly produced by conduction current in Earth's core ($\mathbf{J}_c = \nabla \times \mathbf{H}_c$). The crustal field is mainly produced by magnetization current ($\mathbf{C}_x = \nabla \times \mathbf{M}_x$) in the portion of the lithosphere lying gravitationally above, but thermally below, the Curie isotherm. Within this magnetic crust, part of the magnetization is induced by the present core field and is parallel to \mathbf{B}_c ($\mathbf{M}_{ind} = \chi \mathbf{H}_c$ for susceptibility χ); however, thermoremanent, viscous, chemical, and detrital magnetizations also contribute to \mathbf{M}_x .

At time t and position r in geocentric spherical polar coordinates (radius r , colatitude θ , and east longitude ϕ), the spherical harmonic expansion of zero mean V_{int} is well-known to be

$$V_{\text{int}}(r,t) = a \sum_{n=1}^{\infty} \left(\frac{a}{r}\right)^{n+1} \sum_{m=0}^n [g_n^m(t)\cos m\phi + h_n^m(t)\sin m\phi] P_n^m(\cos\theta), \quad (1d)$$

where P_n^m is the Schmidt-normalized associated Legendre function of degree n and order m and $[g_n^m(t), h_n^m(t)]$ are Gauss coefficients at the reference sphere of radius a (about 6371 km). Gauss coefficients can be estimated by a weighted least squares fit to geomagnetic data; this usually requires truncating the sum over n at finite degree N (see, e.g., Langel [1987]).

By (1c), each internal field coefficient is the sum of core and crustal contributions

$$\begin{aligned} g_n^m(t) &= g_{nC}^m(t) + g_{nX}^m(t) \\ h_n^m(t) &= h_{nC}^m(t) + h_{nX}^m(t). \end{aligned} \quad (1e)$$

Mathematical analysis of geomagnetic measurements made on and above Earth's surface cannot uniquely separate core from crustal field coefficients. Geophysical analysis and interpretation of such measurements nonetheless distinguishes core from crustal fields.

1.2 The Spatial Magnetic Power Spectrum

Lowes [1966, 1974] and others (see Cain et al. [1989b]) show the mean square magnetic induction averaged over a sphere of radius r enclosing its sources to be

$$\langle [B(r,t)]^2 \rangle = \frac{1}{4\pi} \int_0^{2\pi} \int_0^{\pi} [B(r,t)]^2 \sin\theta d\theta d\phi = \sum_{n=1}^{\infty} R_n(r,t), \quad (2a)$$

where $R_n(r,t)$ is the mean square field configured in harmonics of degree n averaged over the sphere

$$R_n(r,t) = (n+1) \left(\frac{a}{r}\right)^{2n+4} \sum_{m=0}^n [g_n^m(t)]^2 + [h_n^m(t)]^2. \quad (2b)$$

The values of $R_n(r,t)$ form the spatial power spectrum of the internal magnetic field. Indeed, the magnetic energy density per harmonic degree integrated over the sphere, $2\pi r^2 \mu_0^{-1} R_n(r,t)$, is the discrete (line) spectrum with dimensions of energy per unit length, hence *spatial power* or *force* (SI units of Joules/meter). Although the SI (MKSA) units of $R_n(r,t)$ are (Tesla)², the $R_n(r,t)$ are nonetheless collectively referred to as the spatial magnetic power spectrum. An individual value of $R_n(r,t)$ implies the spatial power at degree n and is thus called a multipole power: R_1 is dipole power, R_2 is quadrupole power, etc.

The exponential attenuation of $R_n(r,t)$ with n ensures convergence of the sum in (2a) at all $r > a$ if the *reference spectrum* at time t ,

$$R_n = (n+1) \sum_{m=0}^n (g_n^m)^2 + (h_n^m)^2 = \lim_{r \rightarrow a^+} R_n(r), \quad (2c)$$

is of finite power law form ($R_n \leq Kn^\alpha$ for finite α). Divergence of a summed reference spectrum $\sum_n R_n$ merely indicates sources at $r \geq a$, such as those due to Earth's ellipticity and surface topography (e.g.,

magnetization of Mount Kilimanjaro). Curiously, crustal sources above the reference sphere imply that (1d) alone is not enough to represent the field on Earth's aspherical surface due to sources within the Earth. This particular complication in representing the field does not arise at satellite altitudes.

1.3 Core and Crustal Spectra

As core and crustal magnetic fields change with time, numerical values of core and crustal coefficients realized during a very long interval of geologic time define two populations of coefficients (two ensembles). Statistical properties of these populations can be estimated by analysis of geoleomagnetic observations and used to test theoretical predictions derived from geophysical hypotheses. Such predictions may involve probability distribution functions (PDFs) for the coefficients or functions thereof, notably expectation values. An expectation value of a quantity q , denoted $\{q\}$, is the integral of q multiplied by a PDF for q over all possible q . The correlation between two quantities p and q is the normalized covariance $\{(p - \{p\})(q - \{q\})\}(\{p^2\}\{q^2\})^{-1/2}$.

To the extent that core and crustal coefficients are uncorrelated and of zero expectation value,

$$\begin{aligned} \{(g_n^m)^2\} &= \{(g_{nc}^m + g_{nx}^m)^2\} = \{(g_{nc}^m)^2\} + \{2g_{nc}^m g_{nx}^m\} + \{(g_{nx}^m)^2\} \\ &= \{(g_{nc}^m)^2\} + \{(g_{nx}^m)^2\}. \end{aligned} \quad (3a)$$

A similar relation holds for $\{(h_n^m)^2\}$. To the extent that (3a) holds, the expected total spectrum $\{R_n\}$ is the sum of expected core and crustal spectra,

$$\{R_n\} \approx \{R_{nc}\} + \{R_{nx}\}. \quad (3b)$$

Equation (3a) implies (3b), but equation (3b) does not imply (3a) because of the sum over harmonic order implicit in (3b). Indeed, (3b) can be an excellent approximation, even if some core and crustal coefficients are strongly correlated, provided the $2n+1$ cross correlations, which may be either positive or negative, tend to cancel when summed over order m (e.g., $\{g_{nc}^6 g_{nx}^6\} = -\{g_{nc}^7 g_{nx}^7\} \neq 0$). So (3b) is less restrictive than (3a). It may thus seem reasonable to suppose that

$$R_n \approx R_{nc} + R_{nx}. \quad (3c)$$

Given (3b) alone, a particular set of cross terms (like $2g_{nc}^m g_{nx}^m$) for a particular degree n amounts to $2n+1$ samples of a population with zero mean. If these samples are random, then the relative error in (3c) ($|R_n - R_{nc} - R_{nx}|/R_n$) is expected to fall off in proportion to $(2n+1)^{-1/2}$ by the central limit theorem. For example, the expected relative error in (3c) would be $\leq 20\%$ for $n \geq 12$.

Expectation operators are linear operators; therefore, in regions where (2a) and (2b) hold, (3b) implies

$$\begin{aligned} \langle B^2 \rangle &= \langle B_c^2 \rangle + \langle 2B_c \cdot B_x \rangle + \langle B_x^2 \rangle \\ &= \langle B_c^2 \rangle + \langle B_x^2 \rangle. \end{aligned} \quad (3d)$$

Equation (3d) also holds to the extent that the core and crustal fields are uncorrelated *in the mean*; it is less restrictive than (3b) due to the implicit sum over degree and, in turn, is much less restrictive than (3a). Of course, $2B_c \cdot B_x$ varies from place to place and typically dominates the scalar anomaly $|B| - |B_c|$ mapped by many magnetic surveys because $|B_c| \gg |B_x|$. Provided B_c is dominated by low degree, broad scale structure and B_x is dominated by high degree, narrow scale structure, orthogonality of the spherical harmonics ensures that $|\langle 2B_c \cdot B_x \rangle| \ll \langle |2B_c \cdot B_x| \rangle$ on the reference sphere.

1.4 The Core Spectrum

According to the famous interpretation of the spatial magnetic power spectrum derived from MAGSAT by Langel & Estes [1982], the core field dominates R_n for degrees $n \leq 12$ and the crustal field dominates R_n for $n \geq 16$. For degrees $1 < n \leq 12$, and apparently $1 \leq n \leq 12$, the spatial magnetic power spectrum is well described by McLeod's Rule for the core field [McLeod, 1985; 1994, 1996 equation (20)].

In a simplified derivation of McLeod's Rule for finite degrees n [Voorhies & Conrad, 1996], random geomagnetic secular variation ($\partial_t \mathbf{B}$) is induced by fluid motion near the top of a roughly spherical, high conductivity core of mean radius c . The spatial power spectrum for such secular variation is expected to be that of local differential dipole moments of random orientation and random moment

$$F_{nc}(c) = (n+1) \left(\frac{a}{c}\right)^{2n+4} \sum_{m=0}^n (\partial_t g_{nc}^m)^2 + (\partial_t h_{nc}^m)^2 \quad (4a)$$

$$\approx \{F_{nc}(c)\} = C n (n+1/2) (n+1), \quad (4b)$$

(c.f. section 2.2). The variation at the top of the free-stream must, however, diffuse through a thin viscous boundary layer separating the free-stream from the electrically resistive mantle (see Appendix A). The diffusive time-scales τ_n depend upon the effective scale heights $(\pi k_{rn})^{-1}$ for poloidal field harmonics within the core, as well as core conductivity σ , and are

$$\tau_n \equiv (\{R_{nc}\} / \{F_{nc}\})^{1/2} = \mu\sigma(\pi k_{rn})^{-2} \quad (4c)$$

(see (A7)). The effective scale heights are taken to be directly proportional to the horizontal length scales, $k_{rn}^{-1} \propto k_{hn}^{-1} \equiv c[n(n+1)]^{-1/2}$, and the consequences for τ_n^2 verified empirically [Voorhies & Conrad, 1996]. Combining this relation with (4c) and (4b) yields

$$R_{nc}(c) = \{R_{nc}(c)\} = K' \frac{n+1/2}{n(n+1)} \quad (4d)$$

$$\approx K' / (n+1/2), \quad (4e)$$

which, upon upward continuation, is McLeod's Rule. For degrees $n \leq 12$, the implied contribution to the reference spectrum is

$$R_{nc} = \{R_{nc}(a)\} \approx K' (n+1/2)^{-1} (c/a)^{2n+4} \quad (4f)$$

Geophysical parameters $c = 3.5$ Mm and $K' = 5.5 \times 10^{10}$ nT² in (4f) are determined empirically via analysis of geomagnetic observations.

Voorhies & Conrad [1996] used McLeod's Rule and ancillary hypotheses to accurately predict (i) the mean radius of Earth's core; (ii) mean paleomagnetic field intensity; and (iii) the mean rates and mean durations of major geomagnetic dipole power excursions and durable reversals of Earth's axial dipole. The predicted core radius is within 1% of the seismologic value ($c_s = 3480$ km). The predicted mean paleomagnetic intensity is well within the broad range of experimental mean values. The predicted mean reversal frequency (2.26/Ma) is within 3% of the paleomagnetic mean value for the past 84 million years. Again, the core field spectrum is well described by McLeod's Rule.

1.5 A Level Crustal Spectrum?

By analogy with Lowes [1974], when the $R_n(r)$ for some range of n are approximated by the exponential $R_n^*(r) = A^* (b^*/r)^{2n+4}$, linear regression through observational values of $\ln[R_n(a)]$ calculated from a geomagnetic field model gives

$$\ln[R_n^*(a)] = n[\ln(b^*/a)^2] + [\ln(A^*) + 4\ln(b^*/a)]. \quad (5)$$

The slope of this line implies the radius b^* at which the model spectrum $R_n^*(r)$ becomes independent of n (or "levels off"). If R_n^* is extrapolated to arbitrarily high degree, then the sum over n of $R_n^*(r)$ diverges for $r \leq b^*$; therefore, such extrapolation is not valid below b^* . This might be due to failure of the potential field representation, so b^* might be the minimum radius of a sphere containing the sources.

The Langel and Estes [1982] fitted two spectra of form (5) to the R_n spectrum from their degree 23 model MGST 10/81 of Magsat data, one for the core field and one for the crustal field. Their core spectrum levels off 174 km below c . Their crustal spectrum ($R_{nx}^*(a) = 37.1(0.974)^n \text{ nT}^2$) levels off 83 km below a .

Voorhies [1984] fitted the mean square radial field component alone ($B_m^2 = (n+1) R_n / (2n+1) \approx R_n/2$) from MGST 10/81. His core spectrum levels off 200 km below c ; his crustal spectrum ($B_{rx}^2(n) = 11.91(0.9969)^n \text{ nT}^2$) levels off 9.9 km below a . This may suggest upper crustal, rather than deep lithospheric, sources.

Cain et al. [1989b] used their degree 63 model M07AV6 of Magsat data [Cain et al., 1989a] to obtain a core spectrum that levels off about 76 km below c ; a crustal spectrum ($R_{nx}^*(a) = 19.1(0.996)^n \text{ nT}^2$) that levels off 14 km below a ; and an estimated noise level of 0.091 nT^2 .

The results of these analyses are clearly consistent with lithospheric sources for the internal field of degrees 16 or more. More sophisticated crustal magnetic spectra advanced by McLeod and Coleman [1980], Jackson [1990, 1994], and McLeod [1994, 1996], however, indicate substantial modification of the plain exponential form.

2. Theoretical Magnetic Spectra for Thin Spherical Shells

Consider the crustal magnetic field $\mathbf{B}_x = -\nabla V_x$ caused by all K magnetic domains within Earth's magnetic crust. These domains may be considered microscopic rock magnetic domains within the mineral grains comprising Earth's crust; however, the formalism is the same if each domain represents a macroscopic geologic structure. At altitudes above Earth's surface exceeding several times the domain size, each domain $k = 1, 2, 3, \dots, K$ produces a field that can be fairly well described by that of a point magnetic dipole of moment $\mathbf{m}^k \equiv \mathbf{M}^k/\mu_0$ at domain position \mathbf{r}_k . The total crustal potential at observation position \mathbf{r} is thus treated as the superposition of K offset dipole potentials V_x^k ,

$$V_x(\mathbf{r}) = \sum_{k=1}^K V_x^k(\mathbf{r}) = -\sum_{k=1}^K \frac{\mathbf{M}^k}{4\pi} \cdot \nabla \frac{1}{|\mathbf{r} - \mathbf{r}_k|} \quad (6a)$$

$$= \sum_{k=1}^K \frac{\mathbf{M}^k}{4\pi} \cdot \nabla^* \frac{1}{|\mathbf{r} - \mathbf{r}_k|}. \quad (6b)$$

In (6a) and henceforth "M" represents normalized dipole moment, not magnetization. The SI (MKSA) units of \mathbf{M} are Tesla meter³ (Tm^3). In (6b), ∇^* represents the gradient operator written in terms of, and acting on, \mathbf{r}_k coordinates (r_k, θ_k, ϕ_k). The spherical harmonic expansions for the V_x^k are used to rewrite (6a,b) above the crust as

$$V_x(\mathbf{r}) = \sum_{k=1}^K a \sum_{n=1}^{\infty} \left(\frac{a}{r}\right)^{n+1} \sum_{m=0}^n [A_{nk}^m \cos m\phi + B_{nk}^m \sin m\phi] P_n^m(\cos\theta). \quad (6c)$$

To find the coefficients (A_{nk}^m , B_{nk}^m) for moment M^k , recall that

$$\frac{1}{|\mathbf{r} - \mathbf{r}^k|} = \sum_{n=0}^{\infty} \sum_{m=0}^n \frac{(r_k)^n}{r^{n+1}} [C_n^m(\theta, \phi) C_n^m(\theta_k, \phi_k) + S_n^m(\theta, \phi) S_n^m(\theta_k, \phi_k)], \quad (7)$$

where $C_n^m \equiv \cos m\phi P_n^m(\cos\theta)$ and $S_n^m \equiv \sin m\phi P_n^m(\cos\theta)$ (see, e.g., Jackson [1975, equation (3.70)] or Langel [1987, (195)]). Using (7) to evaluate the gradient in (6b), and equating the result with (6c), gives

$$A_{nk}^m = \frac{1}{4\pi a^3} \left(\frac{r_k}{a}\right)^{n-1} [M_r^k n C_n^m(\theta_k, \phi_k) + M_\theta^k \frac{\partial}{\partial \theta_k} C_n^m(\theta_k, \phi_k) - M_\phi^k \frac{m}{\sin \theta_k} S_n^m(\theta_k, \phi_k)] \quad (8a)$$

$$B_{nk}^m = \frac{1}{4\pi a^3} \left(\frac{r_k}{a}\right)^{n-1} [M_r^k n S_n^m(\theta_k, \phi_k) + M_\theta^k \frac{\partial}{\partial \theta_k} S_n^m(\theta_k, \phi_k) + M_\phi^k \frac{m}{\sin \theta_k} C_n^m(\theta_k, \phi_k)], \quad (8b)$$

where (M_r^k , M_θ^k , M_ϕ^k) are the components of M^k .

Detailed models of the phase information

$$g_{nx}^m = \sum_{k=1}^K A_{nk}^m, \quad h_{nx}^m = \sum_{k=1}^K B_{nk}^m \quad (9a)$$

are not needed to derive theoretical forms for the expected crustal magnetic spectrum

$$\{R_{nx}(r)\} = (n+1) \left(\frac{a}{r}\right)^{2n+4} \left\{ \sum_{m=0}^n (g_{nx}^m)^2 + (h_{nx}^m)^2 \right\} \quad (9b)$$

$$= \{R_{nx}\} (a/r)^{2n+4} \quad (9c)$$

implied by simple statistical hypotheses about the K domain dipoles. Indeed, by (9a-c), the reference spectrum for the crustal field produced by these sources is expected to be

$$\{R_{nx}\} = (n+1) \left\{ \sum_{m=0}^n \left(\sum_{k=1}^K A_{nk}^m \right)^2 + \left(\sum_{k=1}^K B_{nk}^m \right)^2 \right\} \quad (10a)$$

$$= (n+1) \left\{ \sum_{m=0}^n \left[\sum_{k=1}^K \sum_{i=1}^K (A_{nk}^m A_{ni}^m) + (B_{nk}^m B_{ni}^m) \right] \right\}. \quad (10b)$$

The functional dependence of the coefficients in (10a,b) upon the domain dipole moments is given by (8a,b). Detailed models (9a) are, however, required to test statistical hypotheses about crustal magnetization by comparing expected spectra (10a,b) with observational spectra (2b) (see section 6).

2.1 Spectrum of a Single Offset Dipole

The magnetic spectrum of a single point dipole $M^k(r_k)$ is

$$R_{nk}(r) = (n+1) \left(\frac{a}{r}\right)^{2n+4} \sum_{m=0}^n (A_{nk}^m)^2 + (B_{nk}^m)^2. \quad (11)$$

By (8a,b), the sum over order m in (11) is

$$\begin{aligned} \sum_{m=0}^n (A_{nk}^m)^2 + (B_{nk}^m)^2 &= G_n \sum_{m=0}^n (M_r^k)^2 n^2 [P_n^m]^2 + G_n \sum_{m=0}^n (M_\theta^k)^2 \left[\frac{d}{d\theta_k} P_n^m \right]^2, \\ &+ G_n \sum_{m=0}^n (M_\phi^k)^2 \frac{m^2}{\sin^2 \theta_k} [P_n^m]^2 + G_n \sum_{m=0}^n M_r^k M_\theta^k n [P_n^m] \frac{d}{d\theta_k} P_n^m \end{aligned} \quad (12)$$

where $G_n(r_k) \equiv (4\pi a^3)^{-2} (r_k/a)^{2n-2}$ and it is understood that both P_n^m and its derivative are evaluated at $\cos \theta_k$.

To cast (11) into a more illuminating function of M^k , five harmonic identities (13a-e) are used to reduce the four sums over m on the right of (12). For arbitrary (θ, ϕ) , the sum rule for the Schmidt normalized harmonics

$$\sum_{m=0}^n [C_n^m(\theta, \phi)]^2 + [S_n^m(\theta, \phi)]^2 = \sum_{m=0}^n (P_n^m)^2 = 1 \quad (13a)$$

(see, e.g., Jackson [1975, equation (3.62) with $\gamma = 0$] or Langel [1987]) is repeatedly differentiated with respect to θ to obtain

$$\sum_{m=0}^n 2 \left[\frac{d}{d\theta} P_n^m \right] [P_n^m] = 0 \quad (13b)$$

$$\sum_{m=0}^n 2 \left[\frac{d^2}{d\theta^2} P_n^m \right] [P_n^m] + 2 \left[\frac{d}{d\theta} P_n^m \right]^2 = 0. \quad (13c)$$

The first sum (of radial terms) on the right of (12) is $(M_r^k)^2 n^2$ by (13a); the fourth sum (of cross terms) is zero by (13b).

To reduce the second sum (of colatitudinal terms) on the right of (12), recall that for either C_n^m or S_n^m the surface Laplacian is

$$\nabla_s^2 S_n^m = -n(n+1) S_n^m = \frac{1}{\sin \theta} \frac{\partial}{\partial \theta} \sin \theta \frac{\partial S_n^m}{\partial \theta} + \frac{1}{\sin^2 \theta} \frac{\partial^2 S_n^m}{\partial \phi^2},$$

$$\frac{d^2 P_n^m}{d\theta^2} = [-n(n+1) + \frac{m^2}{\sin^2 \theta}] P_n^m - \frac{\cos \theta}{\sin \theta} \frac{dP_n^m}{d\theta},$$

so

$$\sum_{m=0}^n \left[\frac{d^2}{d\theta^2} P_n^m \right] P_n^m = \sum_{m=0}^n \left[\frac{m^2}{\sin^2 \theta} - n(n+1) \right] [P_n^m]^2 - \frac{\cos \theta}{\sin \theta} \left[\frac{dP_n^m}{d\theta} \right] [P_n^m].$$

The last terms on the right of this expression sum to zero by (13b); substituting the remainder into (13c) gives

$$\sum_{m=0}^n \left[\frac{d}{d\theta} P_n^m \right]^2 = \sum_{m=0}^n \left[n(n+1) - \frac{m^2}{\sin^2\theta} \right] [P_n^m]^2. \quad (13d)$$

The sum over m of $[m(P_n^m)/\sin\theta]^2$ is needed to reduce third sum on the right of (12) as well as to complete reduction of the colatitudinal terms. To obtain this sum, recall that, with γ being the angle between the position vector to the observation point r and the position vector to the source r_k

$$\cos\gamma = \cos\theta\cos\theta_k + \sin\theta\sin\theta_k\cos(\phi - \phi_k),$$

the full addition theorem for the Schmidt normal harmonics is

$$\sum_{m=0}^n C_n^m(\theta, \phi) C_n^m(\theta_k, \phi_k) + S_n^m(\theta, \phi) S_n^m(\theta_k, \phi_k) = P_n(\cos\gamma),$$

where P_n is the Legendre polynomial of degree n . Repeated operation with $(\sin\theta_k)^{-1} \partial / \partial \phi_k$ gives

$$\sum_{m=0}^n \frac{-m^2}{\sin^2\theta_k} [C_n^m(\theta, \phi) C_n^m(\theta_k, \phi_k) + S_n^m(\theta, \phi) S_n^m(\theta_k, \phi_k)] = \frac{1}{\sin^2\theta_k} \frac{\partial^2 P_n(\cos\gamma)}{\partial \phi_k^2}$$

which, when evaluated at $\gamma = 0$, is the desired sum. Because

$$\frac{\partial^2 P_n(\cos\gamma)}{\partial \phi_k^2} = \frac{d^2 P_n(\cos\gamma)}{d\cos\gamma^2} \left[\frac{\partial \cos\gamma}{\partial \phi_k} \right]^2 + \frac{dP_n(\cos\gamma)}{d\cos\gamma} \frac{\partial^2 \cos\gamma}{\partial \phi_k^2},$$

and noting that

$$\frac{1}{\sin^2\theta_k} \frac{\partial \cos\gamma}{\partial \phi_k} = \sin\theta (\sin\theta_k)^{-1} \sin(\phi - \phi_k)$$

is zero at $\gamma = 0$ while

$$\frac{1}{\sin^2\theta_k} \frac{\partial^2 \cos\gamma}{\partial \phi_k^2} = -\sin\theta (\sin\theta_k)^{-1} \cos(\phi - \phi_k)$$

is -1 at $\gamma = 0$, the desired sum reduces to

$$\begin{aligned} \sum_{m=0}^n \frac{-m^2}{\sin^2\theta_k} [P_n^m(\cos\theta_k)]^2 &= -\frac{dP_n(\cos\gamma)}{d\cos\gamma} \Big|_{\gamma=0} \\ &= -dP_n(x)/dx \Big|_{x=0} = -n(n+1)/2. \end{aligned} \quad (13e)$$

In (13e), x denotes $\cos\theta$ and the final step follows from the Legendre equation at $x = 0$ and the usual normalization of Legendre polynomials ($P_n(0) = 1$).

By (13e), (13d) is equal to $n(n+1)/2$. The second sum on the right of (12) is thus $n(n+1)(M_\theta^k)^2/2$. Moreover, by (12e), the third sum (of longitudinal terms) on the right of (12) is $n(n+1)(M_\phi^k)^2/2$. Substitution of (12), as simplified via identities (13a-e), into (11) yields

$$R_{nx}^k(r) = \frac{1}{(4\pi r^3)^2} \left(\frac{r_k}{r}\right)^{2n-2} [n^2(n+1)(M_r^k)^2 + \frac{1}{2} n(n+1)^2 [(M_\theta^k)^2 + (M_\phi^k)^2]] . \quad (14)$$

Equation (14) gives the spatial magnetic power spectrum on the sphere of radius r due to a point dipole of moment M^k located inside the sphere at position r_k . Note that there is no radius at which (14) becomes independent of degree n . Compared with the plain exponential spectrum that levels off at radius r_k ($R_n^* = A^*(r_k/r)^{2n+4}$), the spectrum of an offset dipole increases as a cubic polynomial of n .

Spectrum (14) is insensitive to the north-south vs. east-west orientation of a dipole because $R_n(r)$ is invariant under rotations of the coordinate system. Yet a well-offset radial dipole can produce almost twice the mean square field ($\Sigma_n R_n(r)$) of a horizontal dipole because $R_n(r)$ does vary under coordinate translations. This seems intuitively obvious in light of the inverse cube law and the anisotropy whereby, at a fixed distance from a dipole, field intensity on its axis is twice that on its equator. The area of strong field intensity directly above a well-offset radial dipole clearly dominates the mean square field on the sphere. For a horizontal dipole of the same absolute moment at the same modest depth, there are two areas of strong field on the sphere; however, these areas are further from the dipole itself, have lesser intensity, and thus give a smaller mean square field than does the radial dipole. Of course, a geocentric magnetic dipole of moment m_0 is purely radial and, with $r_k = 0$, equation (14) correctly gives the single non-zero R_n , $R_1 = 2(\mu_0 m_0 / 4\pi r^3)^2$.

2.2 Randomly Oriented Dipoles on a Spherical Shell (Spectrum Iss)

At a particular instant in geologic time, the K domain dipoles are regarded as a sample population with mean square moment $\{M^2\}$. The coefficients appearing in (10) are given in terms of domain dipole moments M^k by (8a,b). The positions of the dipoles are taken to be random samples from a laterally uniform spatial distribution. The positions are thus expected to be uncorrelated in that $\{r_k \cdot r_i\}$ is equal to $\delta_{ki} \{(r_k)^2\}$, where the Kronecker delta δ_{ki} is 1 if $k = i$ and is 0 if $k \neq i$.

If the dipole moments are randomly oriented, then any particular orientation is as likely as its opposite

$$\{M_r^k\} = \{M_\theta^k\} = \{M_\phi^k\} = 0, \quad (15a)$$

there is no reason to expect cross-correlated components for an individual moment

$$\{M_r^k M_\theta^k\} = \{M_r^k M_\phi^k\} = \{M_\theta^k M_\phi^k\} = 0, \quad (15b)$$

there is no reason to expect cross-correlated moments

$$\{M_r^k M_r^i\} = \{M_\theta^k M_\theta^i\} = \{M_\phi^k M_\phi^i\} = 0 \text{ for } k \neq i \quad (15c)$$

$$\{M_r^k M_\theta^i\} = \{M_r^k M_\phi^i\} = \{M_\theta^k M_\phi^i\} = 0 \text{ for } k \neq i, \quad (15d)$$

but the auto-correlations remain perfect

$$\{M_r^k M_r^k\} = \{M_\theta^k M_\theta^k\} = \{M_\phi^k M_\phi^k\} = \{M^2\} / 3. \quad (15e)$$

Equations (15a-e), summarized by $\{M_j^k\} = 0$ and $\{M_j^k M_l^i\} = \{M^2/3\} \delta_{ki} \delta_{jl}$, provide a mathematical statement of the random dipoles hypothesis.

Although M^k depends upon position (θ_k, ϕ_k) , position is independent of M^k ; therefore, in evaluating $\{A_{nk}^m\}$ and $\{B_{nk}^m\}$ via (8a,b), the expectation operator passes right through the harmonic functions of (θ_k, ϕ_k) . For random dipoles the expectation values of the coefficients are thus zero: $\{A_{nk}^m\}$ and $\{B_{nk}^m\}$ are zero by (15a) and (8a-b), so $\{g_{nx}^m\}$ and $\{h_{nk}^m\}$ are zero by (9a). It follows that the expected field components are also zero. Moreover, (15c-d) and (8a-b) imply that contributing coefficients are uncorrelated

$$\{A_{nk}^m A_{ni}^m\} = \{B_{nk}^m B_{ni}^m\} = 0 \text{ for } k \neq i. \quad (16)$$

The expected field vector from random dipoles is zero, but the expected spatial power spectrum, hence the expected field intensity, is not. Substitution of (16) into (10b) yields the expected reference spectrum

$$\{R_{nx}\} = (n+1) \left\{ \sum_{m=0}^n \left[\sum_{k=1}^K (A_{nk}^m)^2 + (B_{nk}^m)^2 \right] \right\}. \quad (17)$$

The order of summations in (17) is reversible, so the expected magnetic spectrum from K random dipoles is the sum of the expected spectrum from each dipole. If all K dipoles are at radius r_x , then (14) and (17) imply

$$\{R_{nx}\}^{Iss} = \frac{K}{(4\pi a^3)^2} \left(\frac{r_x}{a}\right)^{2n-2} [n^2(n+1)\{M_r^2\} + \frac{1}{2}n(n+1)^2\{M_\theta^2 + M_\phi^2\}]. \quad (18)$$

With (15c), (18) simplifies to

$$\{R_{nx}\}^{Iss} = \frac{K \{M^2\}}{3(4\pi a^3)^2} [n(n+1)(2n+1)] \left(\frac{r_x}{a}\right)^{2n-2} \quad (19)$$

This is the reference spectrum expected from K random dipoles of mean square moment $\{M^2\}$ on the shell of radius r_x . With amplitude defined via $A_x^I \equiv (2/3)K\{M^2\}/(4\pi a^3)^2$, (19) is rewritten as

$$\{R_{nx}\}^{Iss} = A_x^I n(n+1/2)(n+1) (r_x/a)^{2n-2} \quad (20a)$$

and the expected magnetic spectrum above the spherical shell is just

$$\{R_{nx}(r)\}^{Iss} = \{R_{nx}\}^{Iss} (a/r)^{2n+4}. \quad (20b)$$

There is no radius at which spectrum (20) becomes independent of degree n . Compared with an exponential spectrum that levels off at r_x , the spectrum expected from a shell of random dipoles increases as a cubic polynomial of spherical harmonic degree n .

Although n is a positive definite integer, the derivative of (20b) with respect to n vanishes when

$$(2n^3 + 3n^2 + n) \ln(r_x/r) = -(3n^2 + 3n + 1/2);$$

therefore, spectrum (20b) has finite extrema if and only if $r_x < r$. To the extent that Earth's magnetic crust resembles a randomly magnetized shell of radius $r_x < a$, its reference spectrum (2c) should resemble (20a). If the positive definite shell depth $d = a - r_x$ is small in that $d \ll a$, then reference spectrum (20a) has a maximum or 'peak' at high spherical harmonic degree $N_{xp} \approx -3/[2\ln(r_x/a)] \approx 1.5(r_x/d)$. With $a = 6371$ km, shell depths of 10 km, 20 km, or 40 km respectively give N_{xp} of 954, 477, or 238.

The geometric attenuation factor makes the degree of the peak of spectrum (20b) decrease as radius r increase. For example, at satellite altitude 450 km above, and a shell 10 km below, the reference sphere, the peak is at harmonic degree 21.

2.3 Random Polarity Field-Aligned Dipoles on a Spherical Shell (Spectrum IIss)

Thermoremanent magnetization (TRM) of volcanic rock cooling in the aperiodically reversing geocentric axial dipole field from the core suggests non-randomly oriented domain dipoles. The crustal magnetic spectrum appropriate to field-aligned domain dipoles derived in this section is for domain dipoles that are either parallel or anti-parallel to the present axial dipole field with equal likelihood. Subsequent reorientation of domain dipoles by crustal deformation, metamorphic remagnetization, sea-floor spreading and continental drift, and/or true polar wander may lead to a crustal spectrum more akin to that derived in the previous section; however, the two spectral forms turn out to be remarkably similar.

If the domain dipoles are not randomly oriented, but are either parallel or anti-parallel to a geocentric axial dipole field, then

$$M_r^k = 2M_o^k \cos\theta_k, \quad M_\theta^k = M_o^k \sin\theta_k, \quad M_\phi^k = 0, \quad (21)$$

and M_o^k can be either positive or negative. With no preferred polarity, each M_o^k is a random sample from a population with zero mean value, $\{M_o^k\} = 0$ and

$$\{M_r^k\} = \{M_\theta^k\} = \{M_\phi^k\} = 0. \quad (22a)$$

For example, the PDF for M_o^k could be symmetric due to remanent acquisition processes that are independent of core dipole polarity which, in turn, is independent of absolute core dipole moment. With no reason to expect cross-correlated polarities, $\{M_o^k M_o^i\}$ is zero for $k \neq i$, so

$$\begin{aligned} \{M_r^k M_\theta^i\} &= \{2M_o^k M_o^i \cos\theta_k \sin\theta_i\} \\ &= 2\{M_o^k M_o^i\} \cos\theta_k \sin\theta_i = 0 \quad \text{for } k \neq i \end{aligned}$$

and the expected cross-correlations are zero

$$\{M_r^k M_\theta^i\} = \{M_r^k M_\phi^i\} = \{M_\theta^k M_\phi^i\} = 0 \quad \text{for } k \neq i \quad (22b)$$

$$\{M_r^k M_r^i\} = \{M_\theta^k M_\theta^i\} = \{M_\phi^k M_\phi^i\} = 0 \quad \text{for } k \neq i. \quad (22c)$$

The auto-correlations remain perfect, but now depend on colatitude

$$\{M_r^k M_r^k\} = 4M_o^2 \cos^2\theta_k \quad (22d)$$

$$\{M_\theta^k M_\theta^k\} = M_o^2 \sin^2\theta_k \quad (22e)$$

$$\{M_r^k M_\theta^k\} = 2M_o^2 \cos\theta_k \sin\theta_k \quad (22f)$$

where M_0^2 is the ensemble average $\{(M_0^k)^2\}$. The latter is independent of position, so the sum of (22d) plus (22e) can be readily integrated over the sphere to obtain $\langle \mathbf{M}^k \cdot \mathbf{M}^k \rangle = 2M_0^2$.

For random polarity field-aligned dipoles the expectation values of the coefficients are again zero: $\{A_{nk}^m\}$ and $\{B_{nk}^m\}$ are zero by (22a) and (8a-b), so $\{g_{nx}^m\}$ and $\{h_{nk}^m\}$ are zero by (9a). The expected field components are again zero. Equations (22b-c) and (8a-b) imply that individual coefficients are uncorrelated (see (16)), so the expected spatial magnetic power spectrum is again given by (17).

From (8a,b), (17), (22) and the supposition that all domain dipoles are on the sphere of radius r_x , one obtains the expected reference spectrum

$$\{R_{nx}\}^{IIss} = G_n(r_x) \{(M_0^k)^2\} \sum_{k=1}^K \sum_{m=0}^n n^2(n+1)[2\cos\theta_k P_n^m]^2 + (n+1)[\sin\theta_k \frac{d}{d\theta_k} P_n^m]^2 + n(n+1) \cos\theta_k \sin\theta_k [P_n^m \frac{d}{d\theta_k} P_n^m] \quad (23a)$$

or, by identities (13a-e),

$$\{R_{nx}\}^{IIss} = G_n(r_x) M_0^2 \sum_{k=1}^K n^2(n+1)[4\cos^2\theta_k] + n(n+1)^2[\sin^2\theta_k]/2 . \quad (23b)$$

With domain positions amounting to random samples from a uniform distribution over the spherical shell, the sum in (23b) over all K positions is equivalent to the average over the sphere multiplied by K

$$\begin{aligned} & \sum_{k=1}^K [n(4\cos^2\theta_k) + (n+1)(\sin^2\theta_k)/2] \\ &= \frac{K}{2} \int_0^\pi [4n\cos^2\theta_k + (n+1)(\sin^2\theta_k)/2] \sin\theta_k d\theta_k \\ &= (K/3)[4n + (n+1)] = (5K/3)(n+1/5); \end{aligned}$$

therefore,

$$\{R_{nx}\}^{IIss} = G_n(r_x) (5KM_0^2/3) n(n+1)(n+1/5) . \quad (23c)$$

With $M_0^2 = \{M^2\}/2$ and amplitude $A_x^{II} = 5K\{M^2\}/[6(4\pi a^3)^2]$, (23c) is rewritten

$$\{R_{nx}\}^{IIss} = A_x^{II} n(n+1/5)(n+1)(r_x/a)^{2n-2} \quad (24a)$$

and the expected magnetic spectrum above the shell is

$$\{R_{nx}(r)\}^{IIss}(r) = \{R_{nx}\}^{IIss} (a/r)^{2n+4} . \quad (24b)$$

Like (20a), reference spectrum (24a) increases as a cubic polynomial of n . Like (20b), *there is no radius at which spectrum (24b) becomes independent of degree n .*

The ratio of the expected spectrum for random polarity field-aligned dipoles (24) to that for randomly oriented dipoles (20) is

$$\{R_{nx}\}^{IIss}/\{R_{nx}\}^{Iss} = (A_x^{II}/A_x^I)[(n+1/5)/(n+1/2)], \quad (25a)$$

which increases by but 2.5% as n is increased from 12 to infinity. This should make it difficult to distinguish between these two source distributions by examining observational values of R_n alone.

Nonetheless, if the sum of the squared domain dipole moments are the same for these two different dipole distributions, then $K\{M^2\}$ in A_x^I is the same $K\{M^2\}$ as in A_x^{II} and

$$\{R_{nx}^{IIss}\}/\{R_{nx}^{Iss}\} = (5/4)[(n+1/5)/(n+1/2)]. \quad (25b)$$

All else being equal, the high degree multipole power from random polarity field-aligned dipoles is thus about 25% more than for randomly oriented dipoles. This is attributed to the nearly radial orientation and typically strong moments $\{2M^2\}^{1/2}$ of field-aligned domain dipoles located near the poles. These contribute more to multipole powers R_n than do randomly oriented dipoles of ordinary strength $\{M^2\}^{1/2}$. The surplus power from the polar regions evidently exceeds the power deficit due to the nearly horizontal orientation and typically weak moments $\{M^2/2\}^{1/2}$ of the dipoles located near the equator.

3. Theoretical Magnetic Spectra for a Spherical Annulus

Earth's magnetic crust is not a spherical shell, so the spectra derived above should be corrected for effects of non-zero crustal thickness and ellipticity. To see the effect of such corrections while staying close to the geologic null hypothesis, the position of each dipole is treated as a random sample from a spatially uniform distribution within a magnetic crust of uniform thickness $2d$.

3.1 Random Dipoles in a Spherical Annulus (Spectrum Isa)

As noted in section 2.2, the expected magnetic spectrum from K random dipoles is the sum of the expected spectrum from each dipole. This remains true if such dipoles are distributed in a spherical annulus of inner radius $r_x - d$ and outer radius $r_x + d$. So (18) is here replaced by

$$\{R_{nx}\}^{Isa} = \frac{\{M^2\}}{3(4\pi a^3)^2} \sum_{k=1}^K \left(\frac{r_k}{a}\right)^{2n-2} n(n+1)(2n+1). \quad (26)$$

The sum over k is equivalent to K times the volumetric mean, so

$$\{R_{nx}\}^{Isa} = \frac{4\pi K\{M^2\}}{3(4\pi a^3)X} n(n+1)(2n+1) \int_{r_x-d}^{r_x+d} \left(\frac{r}{a}\right)^{2n-2} r^2 dr, \quad (27a)$$

$$= \frac{K\{M^2\}}{3(4\pi a^3)^2 X} n(n+1) \left[\left(\frac{r_x+d}{a}\right)^{2n+1} - \left(\frac{r_x-d}{a}\right)^{2n+1} \right] \quad (27b)$$

where the volume of the annulus is $X = (4\pi/3)[(r_x+d)^3 - (r_x-d)^3]$. As anticipated, (27b) reduces to (20a) in the limit as (d/r_x) approaches zero. The alternate form

$$\{R_{nx}\}^{Isa} = \frac{K\{M^2\}}{3(4\pi a^3)X} n(n+1) \left(\frac{r_x+d}{a}\right)^{2n+1} \left[1 - \left(\frac{r_x-d}{r_x+d}\right)^{2n+1} \right] \quad (27c)$$

shows that if the top of the layer is at the reference radius, then expected reference spectrum (27) at very high degree is proportional to n^2 rather than n^3 .

With $r_x + d = a$, $A_x^{Ia} \equiv A_x^I (4\pi a^3/2X)$, and

$$\begin{aligned} \{R_{nx}\}^{Ia} &= A_x^{Ia} n(n+1) \left[1 - \left(\frac{r_x-d}{a}\right)^{2n+1} \right] \\ &= A_x^{Ia} n(n+1) \left[1 - \left(\frac{a-2d}{a}\right)^{2n+1} \right], \end{aligned} \quad (28a)$$

the expected magnetic spectrum above such an annulus is

$$\{R_{nx}(r)\}^{Ia} = \{R_{nx}\}^{Ia} (a/r)^{2n+4}. \quad (28b)$$

Reference spectrum (28a) is equivalent to that obtained by Jackson [1990, equation (21)] using a more elegant method. Note that for a solid ball of random dipoles, the expected magnetic spectrum is directly proportional to $n(n+1)(a/r)^{2n+4}$.

The ratio of thick crustal spectrum (28a) to thin shell spectrum (20a) is the thickness factor

$$T_n = \{R_{nx}\}^{Ia} / \{R_{nx}\}^{Iss} = (4\pi r_x^3/X)(2n+1)^{-1} \left[\left(\frac{a}{r_x}\right)^{2n+1} - \left(\frac{r_x-d}{r_x}\right)^{2n+1} \right]. \quad (29)$$

For small relative thickness $\delta = 2d/r_x \ll 1$ and lower degrees $n \ll \delta^{-1}$, T_n is close to unity and (27) can be approximated by (20). Such approximation fails at higher degrees near or exceeding δ^{-1} . For example, the first, second and third columns of Table 1 list n , $360^\circ/n$, and the values of T_n for a 40 km thick crust obtained with $a = 6371$ km, $r_x = 6351$ km, and $\delta \approx 1/159$. The thickness correction amounts to 10% at degree 120. Therefore, a 40 km crustal thickness might be distinguished from an equivalent source shell depth of 20 km – provided the R_n could be determined with 10% accuracy for degrees through 120. Fitting expected spectrum (28a) to similarly uncertain R_n values from a degree 60 model of satellite data is, however, unlikely to give a very much better estimate of magnetic crustal thickness $2d$ than is fitting (20a) and concluding $2d = 2(a - r_x)$.

3.2 Random Polarity Field-Aligned Dipoles in a Spherical Annulus (Spectrum II_{sa})

For field aligned dipoles of random polarity distributed in a spherical annulus of inner radius $r_x - d$ and outer radius $r_x + d$, the analog of (27) is

$$\{R_{nx}\}^{IIsa} = \frac{5(4\pi K)M_0^2}{3(4\pi a^3)2X} n(n+1/5)(n+1) \int_{r_x-d}^{r_x+d} \left(\frac{r}{a}\right)^{2n-2} r^2 dr, \quad (30a)$$

$$= \frac{5K\{M^2\}}{6(4\pi a^3)X} \frac{n(n+1/5)(n+1)}{(2n+1)} \left[\left(\frac{r_x+d}{a}\right)^{2n+1} - \left(\frac{r_x-d}{a}\right)^{2n+1} \right] \quad (30b)$$

$$= \frac{5K\{M^2\}}{6(4\pi a^3)X} n(n+1) \frac{(n+1/5)}{(2n+1)} \left(\frac{r_x+d}{a}\right)^{2n-2} \left[1 - \left(\frac{r_x-d}{r_x+d}\right)^{2n+1} \right], \quad (30c)$$

Table 1: Sample Thickness and Ellipticity Correction Factors for type I and type II dipoles (T_n based on $a = 6371.000$)

n	$360^\circ/n$	T_n (40km)	Q_n	E_n^I	E_n^{II}	TE_n^I	TE_n^{II}
12	30	1.00091	0.9737	1.00023	0.9857	1.00116	0.9860
18	20	1.00208	0.9611	1.00056	0.9786	1.00267	0.9801
24	15	1.00373	0.9487	1.00103	0.9865	1.00480	0.9748
30	12	1.00586	0.9366	1.00164	0.9718	1.00755	0.9702
36	10	1.00847	0.9248	1.00239	0.9586	1.0109	0.9662
48	7.5	1.0151	0.9021	1.00430	0.9462	1.0196	0.9600
60	6	1.0238	0.8803	1.00676	0.9344	1.0307	0.9561
72	5	1.0344	0.8595	1.00976	0.9234	1.0445	0.9546
90	4	1.0541	0.8301	1.0153	0.9081	1.0702	0.9567
120	3	1.0975	0.7853	1.0271	0.8857	1.1127	0.9715
180	2	1.228	0.7090	1.0605	0.8518	1.302	1.0449
240	1.5	1.425	0.6470	1.107	0.8310	1.577	1.183
300	1.2	1.708	0.5960	1.166	0.8217	1.991	1.402
360	1	2.102	0.5536	1.239	0.8230	2.602	1.728
480	0.75	3.383	0.4876	1.427	0.8549	4.819	2.886
600	0.6	5.767	0.4390	1.680	0.9240	9.667	5.315
720	0.5	10.23	0.4018	2.011	1.0313	20.51	10.51
900	0.4	25.38	0.3598	2.694	1.2728	68.08	32.16

where X is again the volume of the annulus. The form (30c) again shows that, when the top of the layer is at the reference radius, the expected reference spectrum at very high degree is proportional to n^2 . With $r_x + d = a$, $A_x^{IIa} = A_x^{II}(4\pi a^3/2X)$,

$$\{R_{nx}\}^{IIa} = A_x^{IIa} n(n+1) \frac{(n+1/5)}{(n+1/2)} \left[1 - \left(\frac{r_x-d}{a}\right)^{2n+1}\right], \quad (31a)$$

and the expected magnetic spectrum above such an annulus is

$$\{R_{nx}(r)\}^{IIa} = \{R_{nx}\}^{IIa} (a/r)^{2n+4}. \quad (31b)$$

The difference between thick crust spectrum (31) and thin shell spectrum (24) again remains small until harmonic degree n approaches the reciprocal relative thickness ($n \approx r_x/2d$). Indeed, the ratio of these spectra for type II dipoles gives the same crustal thickness factor T_n as for type I dipoles (see (29) and third column of Table 1). This is because any systematic change in the absolute moment of type II dipoles with depth, perhaps due to the increase in the strength of the aligning field, has been omitted for simplicity.

4. Theoretical Magnetic Spectra for a Thin Ellipsoidal Shell

Consider K domain dipoles on an ellipsoid of revolution about the polar axis $r_e(\theta)$. The radius of the k^{th} dipole depends upon colatitude θ_k

$$[r_e(\theta_k)]^2 = b_x^2 (1 - \varepsilon^2 \sin^2 \theta_k)^{-1} = a_x^2 (1 + \gamma^2 \cos^2 \theta_k)^{-1}, \quad (32a)$$

where a_x is the semi-major axis, b_x is the semi-minor axis, ε is the (numerical) eccentricity $\varepsilon^2 = 1 - (b_x/a_x)^2$, and γ is here called the "coeccentricity" $\gamma^2 = (a_x/b_x)^2 - 1 = \varepsilon^2/(1 - \varepsilon^2)$. The eccentricity of oblate spheroidal shell (32a) is here taken to be that of the reference ellipsoid. For the latter, Nerem et al. [1994] give $a_e = 6378.137$ km and $b_e = 6356.7523$ km; therefore, $\varepsilon^2 = 6.694384 \times 10^{-3}$.

The volume of the oblate spheroid is

$$V_e = (2\pi b_x^3/3) \int_0^\pi (1 - \varepsilon^2 \sin^2 \theta)^{-3/2} \sin \theta d\theta = 4\pi a_x^2 b_x/3. \quad (32b)$$

For a_e and b_e above, (32b) gives a volume equal to that of a sphere of radius 6371.001 km. The differential surface area element of the ellipsoidal shell is

$$\begin{aligned} dA_e &= \left[1 + \frac{\varepsilon^4 \sin^2 \theta \cos^2 \theta}{(1 - \varepsilon^2 \sin^2 \theta)^2}\right]^{1/2} [r_e(\theta)]^2 \sin \theta d\theta d\phi \\ &= (1 - \varepsilon^2 \sin^2 \theta)^{-1} [1 - \varepsilon^2 (2 - \varepsilon^2) \sin^2 \theta]^{1/2} [r_e(\theta)]^2 \sin \theta d\theta d\phi \\ &= (1 + \gamma^2 \cos^2 \theta)^{-1} [1 + \alpha^2 \cos^2 \theta]^{1/2} [r_e(\theta)]^2 \sin \theta d\theta d\phi \\ &= (1 + \gamma^2 x^2)^{-1} [1 + \alpha^2 x^2] [r_e(x)]^2 dx d\phi \end{aligned} \quad (32c)$$

where $\alpha^2 = (\gamma^2 + \varepsilon^2)/(1 - \varepsilon^2) = 2\gamma^2 + \gamma^4$ and $x = \cos \theta$. The area of the oblate spheroid is

$$A_e = 2\pi \int_0^\pi \left[1 + \frac{\varepsilon^4 \sin^2 \theta \cos^2 \theta}{(1 - \varepsilon^2 \sin^2 \theta)^2}\right]^{1/2} [r_e(\theta)]^2 \sin \theta d\theta$$

$$= 2\pi a_x^2 + \pi \frac{b_x^2}{\epsilon} \ln\left(\frac{1+\epsilon}{1-\epsilon}\right) \quad (32d)$$

For a_e and b_e cited above, the radius of the sphere with area A_e is 6371.007 km.

4.1 Random Dipoles on an Ellipsoidal Shell (Spectrum I_{es})

Statistical properties of random dipoles are still described by (15). The reference sphere of radius a does not enclose those sources at $b_x \leq r_k \leq a$; yet $R_{nx}^k(a_x)$ is merely $R_{nx}^k(a)(a/a_x)^{2n+4}$ by (14). Combining (14), (17), and (15) now gives

$$\{R_{nx}\}^{Ies} = \frac{\{M^2\}}{3(4\pi a^3)^2} [n(n+1)(2n+1)] \sum_{k=1}^K \left(\frac{r_k}{a}\right)^{2n-2}, \quad (33)$$

where r_k depends upon θ_k by (32a).

The sum over k is equivalent to K times the average over the ellipsoidal shell, so the reference spectrum is

$$\{R_{nx}\}^{Ies} = \frac{2K\{M^2\}4\pi a^2}{3(4\pi a^3)^2 A_e} n(n+1/2)(n+1) I_n; \quad (34a)$$

the expected mean square field per harmonic degree n averaged over a sphere above the shell is

$$\{R_{nx}(r)\}^{Ies} = \{R_{nx}\}^{Ies} (a/r)^{2n+4}; \quad (34b)$$

and, in terms of $x \equiv \cos\theta$, the integral in (34a) is

$$I_n \equiv \int_0^1 \frac{r_e(x)^{2n}}{a} \left[\frac{(1+\alpha^2 x^2)^{1/2}}{(1+\gamma^2 x^2)} \right] dx. \quad (34c)$$

With $[r(x)]^2 = a_x^2/(1+\gamma^2 x^2)$ from (32a),

$$\begin{aligned} I_n &= \left(\frac{a_x}{a}\right)^{2n} \int_0^1 (1+\gamma^2 x^2)^{-n-1} [1+\alpha^2 x^2]^{1/2} dx \\ &\equiv (a_x/a)^{2n} Q_n. \end{aligned} \quad (35)$$

Integrals Q_n were evaluated numerically using Simpson's Rule. An analytic recursion relation that accurately approximates the Q_n is derived in Appendix B.

To correct the spherical shell reference spectrum (19) for ellipticity, simply multiply it by the ellipticity factor

$$E_n^I \equiv \{R_{nx}\}^{Ies}/\{R_{nx}\}^{Iss} = (a/r_x)^{2n-2} (4\pi a^2/A_e) Q_n (a_x/a)^{2n} = (a_x/r_x)^{2n} (4\pi r_x^2/A_e) Q_n. \quad (36)$$

If r_x is chosen such that $4\pi r_x^2 = A_e$, then E_n^I is simply $Q_n (a_x/r_x)^{2n}$ and the increase in $(a_x/r_x)^{2n}$ with n partly compensates the decrease in Q_n .

Table 1 shows values of E_n^I computed using the semi-major and semi-minor axes (a_e, b_e) cited above and the radius r_x of the sphere with area equal to that of the corresponding reference ellipsoid. The columns of Table 1 give: $n, 360^\circ/n, T_n, Q_n, E_n^I = Q_n(a_x/r_x)^{2n}$ from (36) and other terms discussed in following sections. E_n^I exceeds unity because elevating random dipoles on the equatorial bulge adds more to $\{R_{nx}\}$ above the shell, hence to E_n^I , than depressing dipoles near the poles subtracts from it. As anticipated in light of section 3.2, the corrections are appreciable (+17% or more) at harmonic degrees near or exceeding the reciprocal flattening ($n \geq 1/f = a_x/(a_x - b_x) \approx 298$).

4.2 Random Polarity Field-Alligned Dipoles on an Ellipsoidal Shell (Spectrum IIes)

Field alligned domain dipole moments M^k should vary systematically over the oblate spheroidal shell (32a), not only because an alligning geocentric axial dipole field varies with colatitude, but because the $(a/r)^3$ attenuation further weakens such a field on the equatorial bulge and strengthens it on the flattened poles. The latter indicates modification of (21); however, omitted variations in the alligning field (dipole tilt, non-dipole core fields, and temporal changes) are already larger than this effect. Equations (21) and (22a-f) are therefore retained and, with (8a,b) and (10b), the expected spectrum remains the sum of K contributing spectra (17).

As in section 4.1, ellipticity prevents attenuation factor $G_n(r_k) = (4\pi a^3)^{-2} [r_e(\theta_k)/a]^{2n-2}$ from being replaced with $G_n(r_x)$. So (23b) is replaced with

$$\{R_{nx}\}^{IIes} = \frac{M_o^2}{(4\pi a^3)^2} n(n+1) \sum_{k=1}^K \left(\frac{r_k}{a}\right)^{2n-2} [4n \cos^2 \theta_k + (n+1)(\sin^2 \theta_k)/2]. \quad (37a)$$

With (32a) for $r_k = r_e(\theta_k) = r_e(x_k)$ on the ellipsoid,

$$\{R_{nx}\}^{IIes} = \frac{M_o^2}{(4\pi a^3)^2} n(n+1) \left(\frac{a_x}{a}\right)^{2n-2} \sum_{k=1}^K [4nx_k^2 + (n+1)(1-x_k^2)/2](1+\gamma^2 x_k^2)^{1-n}. \quad (37b)$$

Again, the sum is replaced with K times the average over the shell, which amounts to integrating over differential area element (32c) and dividing by the area of the ellipsoidal shell. The resulting reference spectrum

$$\{R_{nx}\}^{IIes} = \frac{2\pi a^2 K \{M^2\}}{(4\pi a^3)^2 A_e} n(n+1) J_n, \quad (38a)$$

with

$$J_n = \left(\frac{a_x}{a}\right)^{2n} \int_0^1 [4nx^2 + (n+1)(1-x^2)/2](1+\gamma^2 x^2)^{-n-1} (1-\alpha^2 x^2)^{1/2} dx$$

$$= \frac{5n+1}{3} \left(\frac{a_x}{a}\right)^{2n} Y_n, \quad (38b)$$

becomes physically meaningful above the shell ($r > a_x$) where

$$\{R_{nx}(r)\}^{IIes} = \{R_{nx}\}^{IIes} (a/r)^{2n+4}. \quad (38c)$$

Comparison of (38a-c) with (23c) shows the ellipticity correction factor for random polarity field aligned dipoles to be

$$E_n^{II} = \{R_{nx}\}^{IIes}/\{R_{nx}\}^{IIss} = (a_x/r_x)^{2n} (4\pi r_x^2/A_e) Y_n. \quad (39)$$

Table 3 shows values of E_n^{II} computed using numerically integrated Y_n , the semi-major and semi-minor axes given above, and $r_x = (A_e/4\pi)^{1/2}$. Unlike E_n^I , correction factor E_n^{II} is less than one for low through intermediate degrees ($n \leq 660$). This is because ellipticity places the stronger, nearly radially oriented domain dipoles near the flattened poles (see section 2.3) and thus further from a source-containing sphere on which the spectrum is evaluated. The corrections are appreciable at harmonic degrees near or exceeding the reciprocal flattening 298 (e.g., -18% at $n=300$). Correction factor E_n^{II} begins to increase with n above this degree and exceeds unity at degree 720. This reflects the dominance of the geometric factor $(a_x/r_x)^{2n}$ at sufficiently high degree: elevation of weaker horizontal domain dipoles on the equatorial bulge ultimately adds more to very high degree multipole power, hence to E_n^{II} , than depressing stronger radial dipoles on the flattened polar caps can subtract from it.

5. Theoretical Magnetic Spectra for an Ellipsoidal Annulus

The expected spatial magnetic power spectrum for an ellipsoidal annulus of either randomly oriented (type I) or random polarity field-aligned dipoles (type II) is here obtained for an oblate layer of invariant eccentricity ϵ and thus slightly variable thickness. In particular, at the top of the shell

$$[r_e^+(\theta_k)]^2 = b_x^2 (1 - \epsilon^2 \sin^2 \theta_k)^{-1} = a_x^2 (1 + \gamma^2 \cos^2 \theta_k)^{-1} \quad (40a)$$

and at the base of the shell of equatorial thickness $2d = a_x - r_e^-(\pi/2)$

$$[r_e^-(\theta_k)]^2 = b_x^{*2} (1 - \epsilon^2 \sin^2 \theta_k)^{-1} = (a_x - 2d)^2 (1 + \gamma^2 \cos^2 \theta_k)^{-1}, \quad (40b)$$

where $b_x^* = (a_x - 2d)(b_x/a_x)$. The volume of this annulus is

$$X_{ea} = (4\pi/3)[a_x^2 b_x - (a_x - 2d)^3 (b_x/a_x)] = 4\pi a_x b_x (2d)[1 + 2d/a_x - (2d^2/a_x)^2/3]. \quad (40c)$$

5.1 Random Dipoles in an Ellipsoidal Annulus (Spectrum I_{ea})

The statistical properties of random dipoles are still described via (15). Combining (14), (17), and (15) again gives (33), but the range of r_k is given by (40a-b). For a spatially uniform distribution of domain dipoles, the sum over K dipoles is replaced by K times the volumetric mean. The differential volume of integration is $dr dA_e$, with dA_e given by (32c); integration over ϕ yields

$$\{R_{nx}\}^{Iea} = \frac{2\pi a^2 K \{M^2\}}{3(4\pi a^3)^2 X_{ea}} n(n+1)(2n+1) \int_{-1}^1 \int_{r_e^-}^{r_e^+} \left(\frac{r}{a}\right)^{2n} \frac{(1 + \alpha^2 x^2)^{1/2}}{(1 + \gamma^2 x^2)} dr dx. \quad (41)$$

Evaluation of the radial integral at the θ dependent limits (40a,b) yields

$$\{R_{nx}\}^{Iea} = \frac{K \{M^2\}}{3(4\pi a^3) X_{ea}} n(n+1) \left(\frac{a_x}{a}\right)^{2n+1} \left[1 - \left(\frac{a_x - 2d}{a_x}\right)^{2n+1}\right] W_n. \quad (42a)$$

where

$$W_n = \int_0^1 [1 + \gamma^2 x^2]^{-n-1} \left[\frac{1 + \alpha^2 x^2}{1 + \gamma^2 x^2} \right]^{1/2} dx. \quad (42b)$$

The ratio of spectrum (42a) for random dipoles in ellipsoidal annulus $[a_x - 2d, a_x]$ to spectrum (27b) for random dipoles in spherical annulus $[r_x - d, r_x + d]$ gives an ellipsoidality factor

$$\frac{\{R_{nx}\}^{Iea}}{\{R_{nx}\}^{Isa}} = (X/X_{ea}) \frac{(a_x)^{2n+1} - (a_x - 2d)^{2n+1}}{(r_x + d)^{2n+1} - (r_x - d)^{2n+1}} W_n. \quad (43)$$

Comparison of the expected reference spectrum for random dipoles in an ellipsoidal annulus (42) with that for random dipoles on a spherical shell (20) leads to the thick ellipsoid factor for type I dipoles,

$$TE_n^I = (4\pi r_x^3 / X_{ea}) (2n + 1)^{-1} (a_x / r_x)^{2n+1} (1 - [(a_x - 2d) / a_x]^{2n+1}) W_n. \quad (44)$$

The seventh column of Table 1 lists TE_n^I computed using $a_x = 6378.137$, $b_x = 6356.7523$ km, and $d = 20$ km as before; however, the radius of the sphere with area equal to that of the ellipsoid with semi-major axis $a_x - d$ is used for $r_x = 6351.03$ km. As anticipated, TE_n^I differs but slightly from the product $T_n E_n^I$.

5.2 Random Polarity Field-Alligned Dipoles in an Ellipsoidal Annulus (Spectrum IIea)

To obtain this final sample spectrum, the sum over K random polarity field alligned domain dipoles in (37a) is again replaced by the volumetric mean over the ellipsoidal annulus. The differential volume element is $dr dA_e$. With dA_e from (32c), evaluation of the ϕ integral gives

$$\begin{aligned} \{R_{nx}\}^{IIes} &= \frac{2\pi a^2 K M_0^2}{(4\pi a^3)^2 X_{ea}} n(n+1) \int_{-1}^1 \int_{r_e^-}^{r_e^+} \left(\frac{r}{a}\right)^{2n} \times \\ &\quad [4nx^2 + (n+1)(1-x^2)/2] \frac{(1 + \alpha^2 x^2)^{1/2}}{(1 + \gamma^2 x^2)} dr dx. \end{aligned} \quad (45)$$

Evaluation of the radial integral at the θ dependent limits (40a,b) yields

$$\{R_{nx}\}^{IIea} = \frac{K M_0^2}{(4\pi a^3) X_{ea}} \frac{n(n+1)}{2n+1} \left(\frac{a_x}{a}\right)^{2n+1} \left[1 - \left(\frac{a_x - 2d}{a_x}\right)^{2n+1}\right] U_n \quad (46a)$$

where

$$U_n = \frac{3}{5n+1} \int_0^1 \frac{4nx^2 + (n+1)(1-x^2)/2}{(1 + \gamma^2 x^2)^{n+1}} \left[\frac{(1 + \alpha^2 x^2)^{1/2}}{(1 + \gamma^2 x^2)} \right] dx. \quad (46b)$$

Comparison of the expected reference spectrum for random polarity, field-alligned dipoles in an ellipsoidal annulus with that for such dipoles on a spherical shell leads to the thick ellipsoid factor for type II dipoles,

$$TE_n^{II} = (4\pi r_x^3 / X_{ea}) (2n + 1)^{-1} (a_x / r_x)^{2n+1} (1 - [(a_x - 2d) / a_x]^{2n+1}) U_n. \quad (47)$$

Table 2: Elementary Spectral Forms $\{R_{nx}\}$ at Reference Radius a .

Type	Description	Form	Amplitude A in $K\{M^2\}/(4\pi a^3)^2$
Flat Spectrum	at radius r_x	$A(r_x/a)^{2n-2}$	Undefined
Random Dipoles			
Iss	Spherical Shell (20)	$A n(n+1/2)(n+1)(r_x/a)^{2n-2}$	2/3
Isa	Spherical Annulus (28)	$A n(n+1)(1 - [(r_x-d)/a]^{2n+1})$	$4\pi a^3/3X$
Isb	Spherical Ball (radius a)	$A n(n+1)$	1
Ies	Ellipsoidal Shell (34)	$A n(n+1/2)(n+1)(a_x/a)^{2n} Q_n$	$(2/3)(4\pi a^2/A_e)$
	or (36)	$A n(n+1/2)(n+1)(r_x/a)^{2n-2} E_n^I$	2/3
Iea	Ellipsoidal Annulus (42)	$A n(n+1)[(a_x/a)^{2n+1} - ((a_x-2d)/a)^{2n+1}] W_n$	$4\pi a^3/3X_{ea}$
	or	$A n(n+1/2)(n+1)(r_x/a)^{2n-2} TE_n^I$	2/3
Ieb	Ellipsoidal Ball	$A n(n+1)(a_x/a)^{2n+1} W_n$	$4\pi a^3/3X_{ea}$
Random Polarity Field-Aligned Dipoles			
IIss	Spherical Shell (24)	$A n(n+1/5)(n+1)(r_x/a)^{2n-2}$	5/6
IIsa	Spherical Annulus (30)	$A n(n+1) \frac{n+1/5}{n+1/2} (1 - [(r_x-d)/a]^{2n+1})$	$(5/4)(4\pi a^3/3X)$
IIsb	Spherical Ball (radius a)	$A n(n+1) \frac{n+1/5}{n+1/2}$	5/4
IIES	Ellipsoidal Shell (38)	$A n(n+1/5)(n+1)(a_x/a)^{2n} Y_n$	$(5/6)(4\pi a^2/A_e)$
	or	$A n(n+1/5)(n+1)(r_x/a)^{2n-2} E_n^{II}$	2/3
IIEa	Ellipsoidal Annulus (46)	$A n(n+1) \frac{n+1/5}{n+1/2} [(\frac{a_x}{a})^{2n+1} - (\frac{a_x-2d}{a})^{2n+1}] U_n$	$(5/4)(4\pi a^3/3X_{ea})$
	or	$A n(n+1/2)(n+1)(r_x/a)^{2n-2} TE_n^{II}$	2/3
IIEb	Ellipsoidal Ball	$A n(n+1) \frac{n+1/5}{n+1/2} (a_x/a)^{2n+1} U_n$	$(5/4)(4\pi a^3/3X_{ea})$

Explanatory Note: For spheres, r_x denotes the radius of a shell of K domain dipoles sources with mean square moment $\{M^2\}$; r_x-d is the radius at the base of a source layer (top at $r_x + d = a$), and X is the volume of the spherical annulus. Sample thickness factors T_n are listed in Table 1. For ellipsoids, a_x is the semi-major axis and A_e is the area of the ellipsoidal shell; X_{ea} is the volume of the constant ellipticity annulus spanning $[a_x-2d, a_x]$. Sample ellipticity factors E_n^I , E_n^{II} are given in Table 1 for $4\pi r_x^2 = A_e$, as are thick ellipsoidal annulus factors TE_n^I and TE_n^{II} .

The eighth column of Table 1 lists TE_n^{II} computed using $a_x = 6378.137$, $b_x = 6356.7523$ km, $d = 20$ km, and $r_x = 6351.03$ km; the latter is the radius of the sphere with area equal to that of the ellipsoid with semi-major axis $a_x - d$. As anticipated, TE_n^{II} differs but slightly from the product of T_n with E_n^{II} .

Table 2 summarizes the elementary theoretical forms the spatial power spectrum of a randomly magnetized crust derived above.

6. Comparison of Theoretical with Observational Spectra

We fitted some of the foregoing theoretically expected forms for the spatial magnetic power spectrum of Earth's crust, $\{R_{nx}(r)\}$, to observational spectra derived via analyses of MAGSAT data, $R_n(r)$. We worked with the $R_n(r)$ computed from the maximum degree $N = 60$ model M102189, and the related $N = 49$ model M102389, derived by Cain, Holter and Sandee [1990]. At the time of our first fits (1994), these models were the state of the art in high degree geomagnetic field analysis. To eliminate any plausible need to correct for core field contributions, only R_n of degrees $n \geq 16$ were fitted. Covariances for these models were not made available, so formally weighted fits were not possible. It was, however, possible to fit $R_n(r)$ at either reference radius $a = 6371$ km ("at the surface") or at radius $a + 420$ km ("at satellite altitude"). The former assigns relatively heavier, and arguably excessive, weight to the higher degree R_n than does the latter. Before summarizing the fits, the derivation of the field models is reviewed to aid understanding of the origin and limitations of the observational R_n .

6.1 High Degree Models of Cain, Holter, and Sandee [1990].

Both M102189 and M102389 are modifications of the model M07AV6 derived by Cain et al. [1989a]. M07AV6 extended an $N = 29$ least squares model to $N = 63$ via numerical integration (Neumann or Gauss-Legendre method). Quiet ($K_p \leq 1^+$), near midnight, Dst corrected, hourly observatory means were used to obtain an improved, degree 10 secular variation (SV) model for reducing data from the 10/79 - 6/80 MAGSAT mission to common epoch. MAGSAT data prior to 11/3/79 or data with $K_p > 2^+$ were rejected, as were 4,478 of 1,330,285 observations that deviated by more than 100 nT from $N = 29$ model M070284. Residuals relative to that model were further corrected for external field effects using (i) a Dst correction for ring current effects and (ii) long wavelength corrections to separated dawn and dusk data as a function of dip latitude for ionospheric and remaining magnetospheric effects.

The corrected residuals were sorted into 3° longitudinal blocks centered about the roots of the degree 64 Legendre polynomials and block mean values of ΔB_r computed. Empty blocks (poleward of MAGSAT ground tracks) were filled by linear interpolation over the pole. Gauss coefficients were computed from the augmented block mean ΔB_r by the usual quadrature in ϕ and Gauss-Legendre quadrature in $\cos\theta$. Coefficients up to $m = 59$ and $n = 63$ were retained; however, coefficients above degree 50 appeared to represent noise [Cain et al., 1989a; 1990]. As noted in section 1.5, Cain et al. [1989b] interpreted the $R_n(r)$ spectrum from model M07AV6 in terms of a 0.091 nT^2 noise spectrum that levels off at 420 km altitude, a crustal spectrum that levels off 14 km below the reference sphere $a = 6371$ km, and a core spectrum that levels off about 80 km below the core surface.

Cain et al. [1990] reexamined the 8 second MAGSAT data set underlying M07AV6 and rejected 22,478, typically high latitude, observations that deviate by more than 50 nT from this model. From the remaining vector component and scalar data, 49,998 were selected to equalize the number of data per $10^\circ \times 10^\circ$ block; 276 values were synthesized from the first 50 degrees of M07AV6 to fill in blocks poleward of the MAGSAT ground tracks. Some abnormalities in the distribution of the resulting 50,274 residuals relative to M07AV6 helped motivate a higher degree least squares spherical harmonic fit to these field values.

Model M102189 was obtained from these values and M07AV6 by keeping coefficients with degrees 51-60 fixed and iterating weighted least squares adjustments (with some modifications in the weights) to coefficients of degrees ≤ 50 (and first degree external terms). The $N = 49$ model M102389 was obtained by a single minor adjustment to a similarly truncated version of M102189. Values of R_n for both models were generously provided by J. Cain [personal communication, 1994].

The coefficients of degrees greater than 50, being those of M07AV6, result from integrating block mean values. Two possible disadvantages to the use of block mean values are noted in passing. First, the calculation of a block mean value filters out information about horizontally narrow scale field structure within the block. Such horizontal averaging should tend to make high degree R_n , as computed from a model fitted to block mean satellite data, *underestimate* true values. Second, the calculation of a block mean value from data acquired in even a thin annulus sampled by a satellite filters out information about the variation of the field with radius in each block. Such information could help establish the degree of contributing fields that fall off as $(a/r)^{n+2}$ for large n . For example, $R_{50}(6371 + 400 \text{ km})$ is 2.15 times $R_{50}(6371 + 450 \text{ km})$. Unlike the horizontal averaging, such radial averaging should tend to make high degree R_n *overestimate* true values. For potential fields, the two effects cancel when the block is replaced with a small spherical ball; yet orbit decay may still cause non-uniform sampling, notably over-sampling of higher altitudes and a tendency for computed R_n to underestimate true values.

6.2 Thin Shell Reference Spectra With No Noise Correction.

The reference spectrum $R_n(a)$ computed from model M102389 [Cain et al., 1990] is shown in Figure 1 as the intersections of short solid line segments. Following Langel & Estes [1982], the spectrum appears dominated by the dipole; a broad scale non-dipole field of deep internal (core) origin for degrees 2 through 12; and fields of crustal origin for degrees 16 and higher. Degrees 13, 14, and 15 are considered transitional. No special significance is attached to the behavior at degrees 2-3 or 8-9 [Voorhies & Conrad, 1996]. The tendency of R_n increase with n above 16 is qualitatively consistent with a crustal origin; indeed, theoretical crustal spectra (20) and (24) show $\{R_{nx}\}$ increasing as n^3 . The tendency for R_n to increase with n is also consistent with the satellite altitude noise level discussed by Cain et al. [1989a,b, 1990].

Plain Exponential Fit. Piecewise exponential representations of a reference spectrum set

$$\ln[R_n^*] = a_0 + a_1 n \quad (48a)$$

for some range of n . By analogy with (5), writing this as

$$\ln[R_n^*] = \ln A^* + (2n+4)\ln(a/r^*) \quad (48b)$$

confirms that such representations level off at radius $r^* = \exp(a_1/2)$ and that $A^* = \exp[a_0 - 4\ln(a/r^*)]$. Although no geophysical significance is here attached to r^* or A^* , the fit of R_n^* to observational R_n does provide background for the study of other spectral forms.

Figure 1 shows the unweighted least squares fit of (48b) to the 34 values of $\ln R_n$ for degrees 16-49 as the long solid line with positive slope. The fit appears close and amounts to

$$R_n^* = 3.5196 (6587.1/6371.2)^{2n+4} nT^2. \quad (49)$$

Spectrum (49) levels off high in the ionosphere, some 216 km above the reference sphere. (This is about half the typical spacecraft altitude and twice the altitude of the ionospheric maximum). The sum of squared residuals

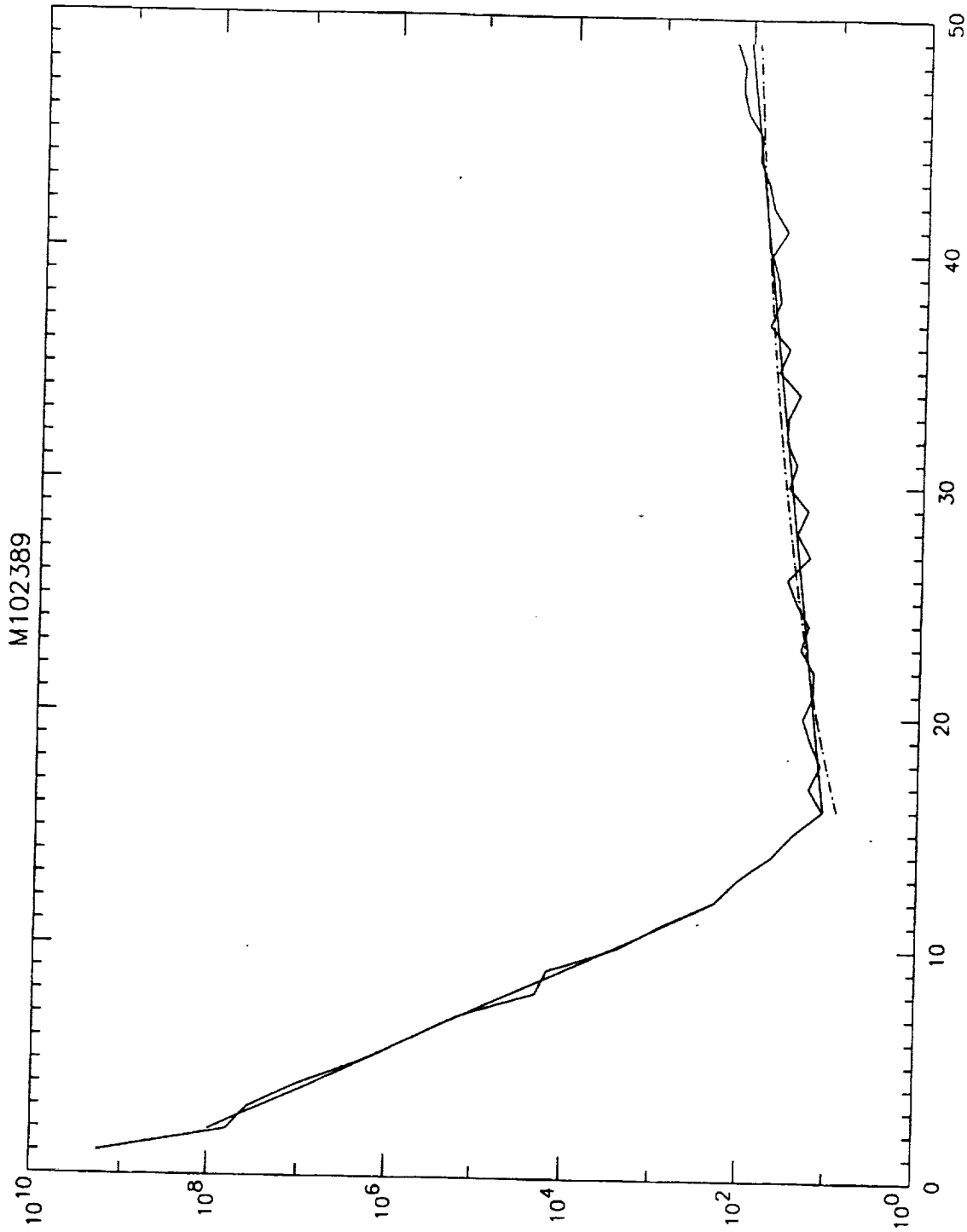


Figure 1. Spatial magnetic power spectrum on the reference sphere, $R_n(a)$ in nT^2 , as a function of harmonic degree n . Short solid lines segments connect observational values from model M102389 of Cain et al. [1990]. Long solid line with positive slope shows plain exponential fitted to degrees 16-49 (linear in $\ln(R_n)$). Dot-dash curve shows spectrum expected from a shell of random dipoles (20) fitted to degrees 16-49.

$$S^2 = \sum_n (\ln R_n - \ln R_n^*)^2 = \sum_n [\ln(R_n/R_n^*)]^2 \quad (50)$$

over the 34 harmonic degrees fitted is 1.630. Without the covariance needed to weight R_n or $\ln R_n$, we are unable to formally test the statistical significance of the residuals. We can, however, compute the scatter factor f , which is the exponential of the root mean square value of $\ln(R_n/R_n^*)$

$$f = \exp[(S^2/34)^{1/2}], \quad (51)$$

and is 1.245. The R_n have been thus been fitted to within a typical factor of $(1.245)^{\pm 1}$. Comparison of the R_n from M102189 with those from M102389, again for degrees 16 through 49, gives the corresponding uncertainty factor $f_0 = 1.0248$. The residuals are therefore much too large to attribute to plausible changes in field model truncation level.

Thin Shell Fits. Figure 1 also shows the fit of expected reference spectrum (20) for randomly oriented dipoles on a shell to the same R_n as the dot-dash curve. In particular, a linear function was least squares fitted to $\ln[R_n n^{-1} (n+1/2)^{-1} (n+1)^{-1}]$ for degrees 16-49 of model M102389. The result,

$$R_n^{Iss} = 2.880 \times 10^{-3} n (n+1/2) (n+1) (6277.1/6371.2)^{2n-2} nT^2, \quad (52)$$

gives a source shell depth of 94 km below the reference sphere. The sum of squared residuals to $\ln R_n$ is now 3.206 and the R_n are fitted to within a typical factor f of $(1.359)^{\pm 1}$. The n^3 dependence of the thin spherical shell spectrum R_n^{Iss} , visible as curvature in Figure 1, produces a fit which is not quite so close as that of plain exponential R_n^* .

The similar fit of expected spectrum (24) for random polarity field aligned dipoles on a shell to the $\ln R_n$ of M102389,

$$R_n^{IIss} = 2.940 \times 10^{-3} n (n+1/5) (n+1) (6276.1/6371.2)^{2n-2} nT^2. \quad (53)$$

gives a source shell depth of 95 km. The S^2 of 3.221 shows that the R_n have been fitted to within a typical factor of $(1.360)^{\pm 1}$. As noted in section 2.2, it is indeed difficult to distinguish between randomly oriented dipoles and random polarity field aligned dipoles from observationally accessible R_n alone.

Table 3 summarizes some spectra fitted to degrees 16-49 of M102389, and to degrees 16-60 of M102189, in columns listing spectral form, model, degree range, key depth, amplitude, and scatter factor. When either random dipoles or random polarity field aligned dipoles spectra are fitted to the higher degree model, the effective shell depth decreases from about 94 km to about 64 km. The shallowing of the source layer compensates the increase in n^3 at the higher degrees (see equations (20), (24)). For the convergent spectral forms, the final column of Table 3 lists the mean square crustal field on the reference sphere obtained by extrapolating the fit,

$$B_x^{rms} = \left[\sum_{n=1}^{100,000} R_n^{Iss} \right]^{1/2} \quad (54)$$

for spectrum I_{ss} and the corresponding sum for spectrum II_{ss} .

A few remarks on Figure 1 and Table 3 are offered. Firstly, the negative depth at which spectrum R_n^* levels off might be physically insignificant because the plain exponential form is unphysical and/or because of noise in the R_n fitted. If the problem is noise, then the slightly closer fit offered by R_n^* is not physically significant. Secondly, the source shell depths from spectra R_n^{Iss} and R_n^{IIss} seem deeper than a mean Curie isotherm, perhaps because these physically motivated forms are inadequate, because of noise in

Table 3: Elementary Spectral Forms Fitted to M102189 & M102389
with no noise adjustment

Form	Model	Degrees	Depth (km)	Amplitude (nT ²)	f	B _x rms (nT)
Exponential	M102389	16-49	-216	3.520	1.245	NA
Exponential	M102189	16-60	-208	3.768	1.251	NA
Iss	M102389	16-49	94.1	2.880×10 ⁻³	1.359	137.23
Iss	M102189	16-60	63.5	2.188×10 ⁻³	1.380	137.56
IIss	M102389	16-49	95.1	2.940×10 ⁻³	1.360	122.73
IIss	M102189	16-60	64.3	2.229×10 ⁻³	1.382	123.03

the R_n fitted, or because of a loss of power from high degree R_n . It turns out that a trade-off between amplitude A and source depth $a-r_x$ makes their coestimation very uncertain.

The extrapolated rms crustal field listed in the final column of Table 3 is about 130 nT. This is the same order of magnitude as background scalar magnetic anomalies inferred from marine and aeromagnetic surveys. Such anomalies mainly measure the crustal field component parallel to the main field, so the total crustal field intensity could be larger than the scalar anomaly (by a factor of $3^{1/2}$ in an isotropic case); however, the rms crustal field ought not be less than the rms scalar anomaly.

To check this 130 nT rms crustal field prediction, we analyzed the "observatory biases" derived with many main geomagnetic field models by R. Langel and others at GSFC. The idea is that each observatory bias approximates the crustal magnetic field at the observatory. R. Baldwin generously provided 10 sets of observatory biases obtained in the course of making 10 somewhat different geomagnetic field models. For each model, each observatory bias ($\Delta B = (\Delta X^2 + \Delta Y^2 + \Delta Z^2)^{1/2}$) was calculated and used to compute the rms bias. The ten rms biases average to 488 ± 106 nT. A very few observatories had very large biases, perhaps due to data errors, site instability, or location on exceptionally magnetic volcanic edifices. Rejecting the few observatory biases over 1500 nT led to 10 rms biases that average to 360 ± 45 nT. The model using the most observatories and longest time span (1900-1995) gave the smallest rms observatory bias of 274 nT. All these values exceed the 130 nT prediction. The sigmas of aeromagnetic (173 nT), repeat (263 nT), and survey (373 nT) data relative to model GSFC(S95-sc) [Sabaka et al., 1997] also exceed the 130 nT prediction. It can thus be argued that the 130 nT prediction for rms crustal field is too low, perhaps by a factor of two or three. This might be due to overestimation of source depth and, in turn, a loss of power from the higher degree R_n fitted.

6.3 Remark on Coestimation of Amplitude, Depth and Thickness

Scatter factors for thin shell spectra I_{ss} and I_{ss} to the observational spectrum (about $(1.36)^{\pm 1}$) exceed the thickness and ellipticity correction factors in Table 1 (which are nearer unity than $(1.07)^{\pm 1}$ for degrees less than 60). This suggests that allowance for thickness and ellipticity ought not appreciably alter the apparent source depth. However, an attempt was made to estimate source layer thickness along with amplitude and depth; this leads to a non-linear inverse problem.

We naively used iterative linearized least squares to fit the spectrum for a thick annulus of random dipoles to observational R_n . The method failed to converge due to an ill-conditioned, almost singular information matrix. As is well known from forward modeling of magnetic anomalies, there is a trade-off between magnetization and thickness of a source layer. In the present context, note that spectrum (27b) can be written

$$\{R_{nx}\}^{I_{sa}} = A_x I_a n(n+1) \left(\frac{r_x}{a}\right)^{2n+1} \left[\frac{2n+1}{(1+d/r_x)} - \frac{2n+1}{(1-d/r_x)} \right] \quad (55a)$$

which, for sufficiently thin layers ($2d \ll r_x$) and low degrees is approximately

$$\{R_{nx}\}^{I_{sa}} \approx A_x I_a n(n+1) \left(\frac{r_x}{a}\right)^{2n} (2n+1)(2d/a). \quad (55b)$$

The partial derivative of (55b) with respect to amplitude $A_x I_a$ is directly proportional to the partial with respect to d ; in practice, the approximate colinearity led to a near singular information matrix.

It was possible to fix layer thickness, estimate amplitude and depth, and then adjust the layer thickness to tighten the fit, but no clearly preferred solution emerged by iterating this procedure.

6.4 Thin Shell Spectra With Noise Correction.

The form of the satellite altitude noise spectrum used by Cain et al. [1989b] is the plain exponential that levels off at 420 km,

$$R_n^e(r) = e [(a + 420\text{km})/r]^{2n+4}. \quad (56)$$

Cain et al. [1989b] averaged the higher degrees ($n > 50$) of $R_n(a + 420\text{km})$ to obtain the noise level $e = 0.091 \text{ nT}^2$. For a degree 60 model, the corresponding rss noise would be $(60e)^{1/2}$, or 2.3 nT. This is about the rss noise expected uniformly distributed attitude errors of at most 20" in the ambient field and so seems plausible; however, it is less than indicated by a Magsat total measurement error budget. It is not clear that attitude, other data errors, or modeling errors such as aliasing should cause a level spectrum (56).

We did not expect to estimate noise level e along with the amplitude and source depth of a crustal spectrum due to colinearity; subsequent experiments verified this colinearity. We bypassed least squares coestimation in favor of mapping misfit as a function of theoretical spectrum parameters (amplitude and depth) at each of several noise levels. The measure of misfit computed was the standard deviation of the theoretical spectrum relative to the noise-adjusted unweighted observational $R_n(r)$ from degrees 16-50 of M102189.

$$\sigma(r) = ([32]^{-1} \sum_{n=16}^{50} [R_n(r) - \{R_{nx}(r)\} - R_n^e(r)]^2)^{1/2}. \quad (57)$$

Contour plots of σ at each noise level show a strong tradeoff between amplitude and depth: a shallower source layer can be accommodated without much change in misfit provided source amplitude is reduced.

Figure 2 shows two examples of such σ plots, both obtained from (56) at reference radius $r = a = 6371 \text{ km}$ and $e = 0.091 \text{ nT}^2$. The upper panel contours the standard deviation, as a function of amplitude A (nT^2) and depth $a-r_x$ (km), when $\{R_{nx}(r)\}$ in (57) represents an ellipsoidal shell of random dipoles (34),

$$\{R_{nx}(a)\} = A n(n + 1/2)(n + 1) Q_n^* [r_x/a]^{2n-2}. \quad (58)$$

A flaw caused Q_n^* to exceed the Q_n in Table 3 by an unimportant 0.23%. Minimum σ (10.91 nT^2) is for a source depth of 45 km; the range of source depths giving $\sigma \leq 11 \text{ nT}^2$ is 20-55 km. This seems almost geophysically plausible; however, the range of source depths giving $\sigma \leq 12$ is far larger. The tradeoff between amplitude and depth is clear in the upper panel of Figure 2.

The lower panel of Figure 2 contours the standard deviation as a function of amplitude and depth, but with $\{R_{nx}(r)\}$ in (57) taken to be the plain exponential spectra $R_n^* = A(r^*/a)^{2n+4}$. The leveling depth $a-r^*$ is negative and σ is minimum (9.57 nT^2) for a leveling altitude of 200 km; however, σ is less than 10 nT^2 for a broad range of altitudes between 265 km and 235 km.

Compared with an exponential spectrum leveling off at 200 km altitude, the modest increase in σ caused by the random dipoles spectrum (20) seems a small price to pay for a 45 km deep crustal source layer. Yet the misfit contoured in Figure 2 is for R_n evaluated on the reference sphere, not at satellite altitude.

With no formal weights for the observational R_n , misfit $\sigma(a)$ is dominated by the deviations at the higher degrees ($n > 40$) due to the geometric amplification upon downward continuation from satellite altitude. To reduce this effect, similar figures were constructed (i) for misfit measured at satellite altitude instead of on the reference sphere and (ii) for degrees 16-40 instead of 16-50. Many noise levels were sampled in both cases. The de-emphasis upon higher degree R_n tends to increase the apparent depth of the

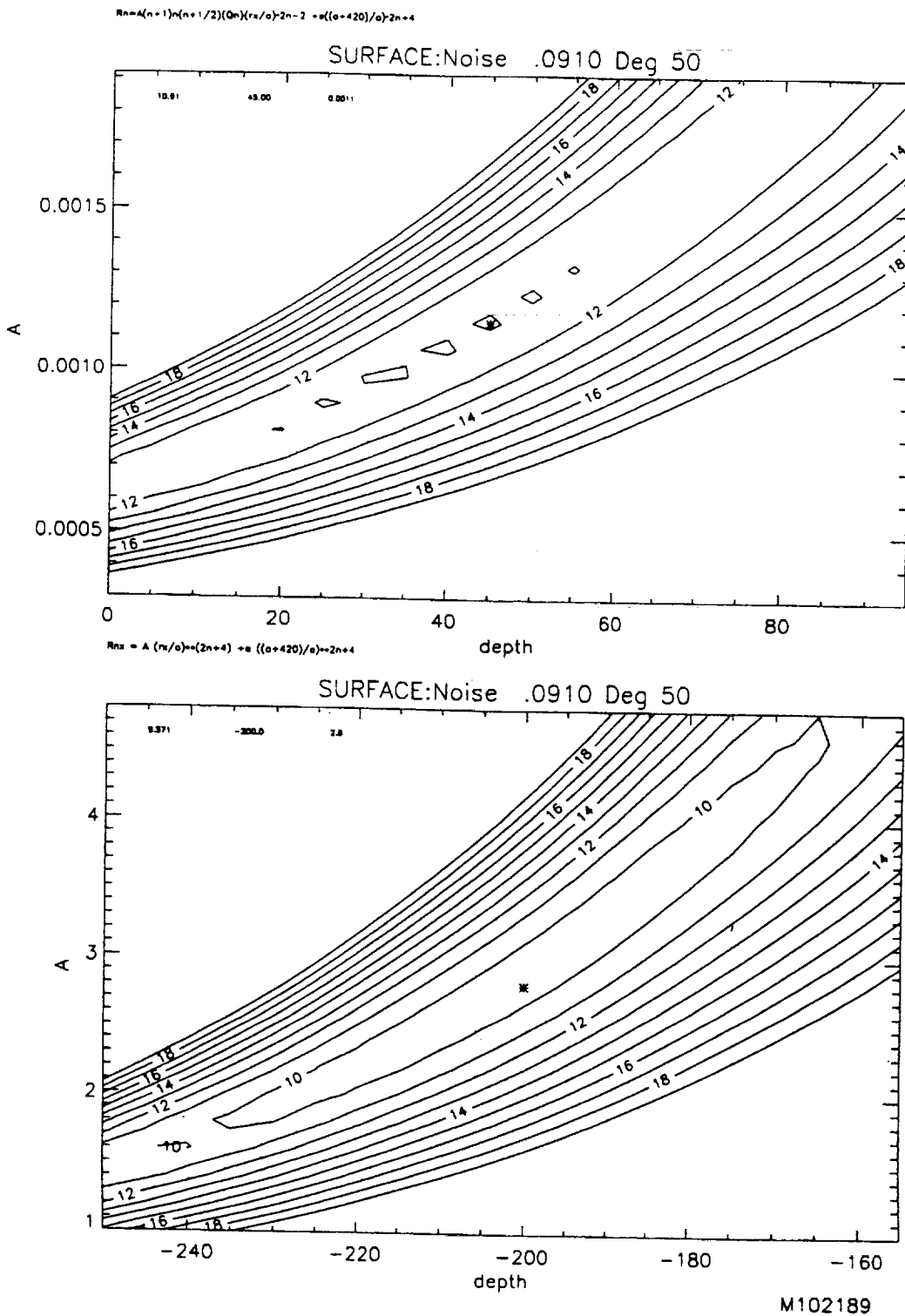


Figure 2. Trade-off surfaces map standard deviation σ as a function of trial spectrum amplitude A (nT^2) and depth (km). Deviations are measured with respect to degrees 16-50 of noise adjusted observational spectrum $R_n(a)$ from model M102189 of Cain et al. [1990]. Upper panel contours σ for trial spectrum expected from an ellipsoidal shell of random dipoles; note minimum σ for shell depths of 20-55 km. Lower panel contours σ for plain exponential trial spectrum; note minimum σ at negative depth (positive altitude) may result from downward continuation of noise.

source layer. The main result is that a very broad range of source depths and noise levels can be accommodated without much change in misfit.

For example, we summarize standard deviations relative to satellite altitude $R_n(a + 420 \text{ km})$, minus noise level $e = 0.091 \text{ nT}^2$, for degrees 16-50 of M102189. The plain exponential spectrum gives $\sigma(a + 420 \text{ km}) \leq 0.1 \text{ nT}^2$ at leveling altitudes between 120 km and 160 km; yet values $\leq 0.2 \text{ nT}^2$ are found in the much broader range between a leveling depth of 80 km and a leveling altitude above 200 km. One local minimum within this range is about 20 km deep - close to the geophysically plausible 14 km leveling depth obtained by Cain et al. [1989b]. In contrast, the ellipsoidal shell of random dipoles (57) only returns $\sigma(a + 420 \text{ km}) \leq 0.2 \text{ nT}^2$ for seemingly implausible shell depths of 60 km or more.

To perform decisive statistical tests needed to reject various theoretical functional forms for the crustal magnetic spectrum, one requires reliable uncertainty estimates not only for observational R_n , but for the theoretical spectrum (e.g., $\{(R_n - \{R_n\})^2\}$). In the interim, geophysically reasonable source models can be preferred to either elementary theoretical forms or arbitrary mathematical functions.

6.5 Spectrum of an Equivalent Source Model of Magsat Crustal Anomalies

Since the identification of magnetic anomalies in Magsat data, many researchers have devoted much effort to develop data processing techniques that help isolate the field of lithospheric origin and improve satellite magnetic anomaly maps for geologic interpretation (see, e.g., Ravat et al. [1995]). One step in some of these techniques involves computing an equivalent source representation of reduced anomaly data. An equivalent source model is a network of point dipoles, typically main field-aligned and located on the reference sphere, with absolute moments distributed so as to reproduce the anomaly data. In practice, the dipoles are closely spaced, albeit fewer in number than the data, and singular value decomposition may be used to avoid unphysical numerical instabilities in a least squares estimate of absolute moments; alternatively, a damped least squares approach may be used.

From one such equivalent source model with a nearly uniform dipole spacing of about 220 km, M. Purucker [1994, personal communication] generously provided values of the radial magnetic component computed at the mesh points of a 2° equiangular grid and 400 km altitude. The spherical harmonic coefficients and equivalent source spectrum $R_n(\text{ES})$ through degree and order 90 were computed from these synthetic data by numerical integration. The spectrum peaks near degree 50, but shows ringing above degree 70 due to source spacing and coarseness of mesh. From apparently reliable degrees 16-55, the standard deviation σ of simple power laws ($R_n(\text{ES}) \approx An^q$) was mapped as a function of amplitude A and index q . Minimum σ was found for $q = 1.55$. Neither a level (n^0) spectrum nor a random dipoles (n^3) spectrum describes the equivalent source crustal anomaly model as well as an intermediate ($n^{3/2}$) form. Whether the particular q value obtained reflects correlations introduced by data reduction and equivalent source modeling procedures or some fundamental property of Earth's magnetic crust is not clear. It is clear that a power law index less than 3 is reasonable for spatially correlated magnetizations.

7. Summary

The magnetic field produced by magnetization in Earth's crust and lithosphere is distinguishable from the field produced by electric currents in Earth's core because the spatial magnetic power spectrum of the crustal field differs from that of the core field. This principle has long guided analyses of land, sea, and aero-magnetic survey data, which routinely subtract a broad scale field - be it a constant level, a regional trend, a long wavelength model, or a low degree geomagnetic reference field model - before attempting geologic interpretation of residual anomalies. According to the famous Langel & Estes [1982] interpretation of the spectrum derived from MAGSAT, the core field dominates the total spectrum, R_n , for

spherical harmonic degrees $n \leq 12$ and the crustal field dominates for $n \geq 16$. Observational spectra exhibit two distinct regimes because the different radii of the two main source regions ($r_c \ll r_x$) cause distinctly different geometric attenuation factors for the core spectrum $(r_c/a)^{2n+4}$ and the crustal spectrum $(r_x/a)^{2n+4}$. The absence of a third spectral regime, apart from the narrow range of core-crustal overlap, indicates that most of Earth's mantle is neither strongly magnetized nor carrying strong electric currents - as expected for hot insulating silicates. The spectral separation of core and crustal fields remains a geophysical distinction; it does not enable a formally unique mathematical separation of core from crustal field by analysis of satellite and/or near surface geomagnetic field measurements.

The geometric attenuation factors are exponential functions of n , so a single exponential can be fairly closely fitted to either low, or to high, degree R_n . The fit returns a radius which coarsely approximates the radius of either Earth's core or Earth's crust, respectively. This fact boosts confidence in the spectral separation. It does not imply that the core spectrum is flat at the top of the core, nor does it imply that the crustal spectrum is flat at the top of the crust. It does suggest that, after allowance for geometric attenuation, core and crustal spectra are sub-exponential functions of n - perhaps ratios of polynomials in n if not simple power laws.

Physical models of core and of crustal sources suggest that exponential spectra should indeed be multiplied or divided by more slowly varying polynomial functions of harmonic degree n . For example, the core spectrum R_{nc} is well described by McLeod's rule (4e): geometrical attenuation of a spectrum that falls off as $1/(n + 1/2)$ atop Earth's core. Elementary spectra for a randomly magnetized crust are listed in Table 2.

7.1 Two Types of Dipoles on a Shell

Elementary theoretical forms for the crustal magnetic spectrum $\{R_{nx}\}$ derived above treat the source of the crustal magnetic field as an ensemble of domain dipoles. The first step derived the spatial magnetic power spectrum on the sphere of radius r due to a point dipole of moment M^k located inside the sphere at position r_k (14). There is no radius at which the spectrum for an offset dipole (14) becomes independent of degree n or levels off. Compared with the exponential spectrum that levels off at radius r_k ($R_n^* = A^*(r_k/r)^{2n+4}$), the spectrum of an offset dipole increases as a cubic polynomial of n .

The second step formulated the geologic null-hypothesis that the magnetic field of Earth's crust is due to many domain dipoles scattered at random throughout a thin crust. Two types of dipole ensembles were considered. Type I, or random, dipoles are of random absolute moment and random orientation; they are not cross-correlated and the auto-correlation matrix is diagonal as described by (15) $\{M_j^k M_l^i\} = \{M^2/3\} \delta_{ki} \delta_{jl}$. Type II, or random polarity field-aligned, dipoles are also of random absolute moment, but are oriented either parallel or anti-parallel to the modern axial dipole field with equal likelihood; they are also not cross-correlated, but the auto-correlation matrix is not diagonal and varies with colatitude as described by (22).

The magnetic spectrum expected from many uncorrelated random dipoles is the sum of the expected spectra from each random dipole. The expected spectrum for type I random dipoles on a spherical shell (20) is thus proportional to that of a single random dipole. *There is no radius at which the expected magnetic spectrum from a shell of random dipoles is independent of degree n .* Compared with the plain exponential that levels off at the shell radius r_x , this spectrum increases as a cubic polynomial of n . The same is true of the expected spectrum for type II random polarity field aligned dipoles (24).

The expectation spectra for type I and type II dipoles prove remarkably similar. Type II dipoles do, however, tend to generate more multipole power - the spectral ratio $\{R_n^{II}\}/\{R_n^I\}$, given by (25) for thin spherical shells, being about 125% for degrees greater than 12. The nearly radial orientation and typically

strong moments of type II dipoles in the polar caps more than makes up for the nearly horizontal orientation and typically weaker moments of type II dipoles in the equatorial belt.

7.2 Crustal Thickness and Ellipticity Corrections

When domain dipoles are scattered throughout a spherical annulus of uniform thickness $2d$, instead of confined to a spherical shell of radius r_x , the shape of the expected spectrum changes. The change amounts to multiplying thin shell spectra by a crustal thickness factor. The factor is quite close to unity at harmonic degrees less than the reciprocal relative thickness of the annulus ($n \leq r_x/2d$). This is in accord with the common geophysical view that the length scale of a source region cannot be established until variations in the exterior potential field of similar scale are resolved. For a 40 km thick annulus, the correction is about 10% at degree 120; therefore, if observational R_n could be determined with 10% accuracy for degrees through 120, a 40 km thick crust might be distinguished from an equivalent source shell depth of 20 km. When fitting models to observational R_n of much lesser degree and/or accuracy, a thick crust model is not likely to return a much better estimate of magnetic crustal thickness than simply doubling the apparent source depth of a thin shell model ($2d = 2a - 2r_x$). In practice, a near co-linearity makes coestimation of amplitude, depth, and thickness difficult or impossible without observational R_n at sufficiently high degrees ($n \approx r_x/2d$).

The expected spectrum from a spherical annulus of either random dipoles (28), or random polarity field aligned dipoles (31), does not level off at any radius. Compared with the plain exponential that levels off at the top of the annulus, these spectra increase as a quadratic polynomial of n at sufficiently high degree ($n \gg a/2d$). This is true for a solid ball of such sources regardless of n .

In deriving expected spectra $\{R_{nx}\}$, the effect of oblateness is somewhat more difficult to include than the effect of uniform thickness. The effect amounts to multiplying the thin shell spectrum by an ellipticity factor. This factor is close to unity for harmonic degrees less than the reciprocal flattening ($n \leq a_x/(a_x - b_x) \approx 298$). For type I dipoles, the factor exceeds unity due to geometric amplification: elevating random dipoles on the equatorial bulge adds more to $\{R_{nx}\}$ than depressing dipoles at high latitudes subtracts from it. For type II dipoles, this geometric effect also causes the ellipticity factor to exceed unity at sufficiently high degrees; however, there is a range of lower degrees for which the type II ellipticity factor is less than unity. The reason is clear: compared to a spherical shell, the nearly radially oriented domain dipoles located near the flattened poles are further from the source-containing sphere on which the spectrum is evaluated. Only at very high degree (about 720 for a terrestrial flattening) can this effect be overcome by the elevation of weaker, nearly horizontal domain dipoles on the equatorial bulge.

The effect of scattering the domain dipoles throughout a thick ellipsoidal annulus amounts to multiplying the spectrum expected for a thin spherical shell by a thick ellipsoid factor TE_n (for either type I or type II dipoles). The factor differs but slightly from the product of thickness and ellipticity factors.

7.3 Comparison of Theoretical and Observational Crustal Spectra.

When downwardly continued to the reference radius (6371 km), the observational magnetic spectrum R_n derived from Magsat data by Cain et al. [1990] tend to increase with degree n for degrees 16 through 60. This conflicts with the notion of an exponential crustal spectrum that levels off at or below the Earth's surface. Following Cain et al. [1989b], the increase in R_n with n may be due to downward continuation of a noise component that gives a level spectrum at satellite altitude. The increase may also be due to, and is expected from, a magnetic field originating in randomly magnetized domains, each acting as a random dipole, scattered throughout Earth's crust. When both the satellite altitude noise correction of Cain et al.

[1989b] and the spectrum expected from a shell of random dipoles are used to describe R_n for degrees 16-50, the standard deviation of the residuals is minimal for an apparent source depth in the 20-55 km range.

Although the covariance needed to weight R_n was not available, higher degrees can be de-emphasized by considering satellite altitude $R_n(a + 420 \text{ km})$ or by truncation at degree 40. So doing tends to lower a source shell of random dipoles to seemingly implausible depths of 60 km or more (with or without the noise correction). It also reduces the leveling altitude of a plain exponential spectrum fitted to noise adjusted R_n . We have yet to encounter a physical reason to suppose a level $R_n(r^*)$ spectrum describes either a geophysical source, measurement error, or modeling error at radius r^* .

The results show that, in the absence of reliable uncertainty estimates, neither an elementary functional form for the crustal spectrum, a source shell depth, nor even a simple leveling depth can be reliably extracted from the field models considered. There is, however, some indication that a priori specification of a spectral form $An^\alpha(r_x/a)^{2n-2}$ with source depth $a-r_x$ in the 0-60 km range would return a power law index α : $0 \leq \alpha \leq 3$. Indeed, analysis of an equivalent source model of Magsat anomalies suggests a crustal reference spectrum that varies approximately as $n^{3/2}$.

7.4 Conclusion

A suitable geologic null-hypothesis for the magnetic field originating in Earth's crust is that it results from an ensemble of uncorrelated domain dipoles, either of random orientation or random polarity, scattered throughout the lithosphere. The spatial magnetic power spectrum due to such a randomly magnetized crust differs from the exponential form describing geometric attenuation with radius above a sphere on which the spectrum is independent of spherical harmonic degree n . For harmonic degrees 16-60 of interest in satellite anomaly studies, the difference amounts to multiplying the exponential spectrum by a factor of n^3 . Mathematically interesting corrections for non-zero uniform crustal thickness and ellipticity are of little or no practical concern in this range; they are important for harmonic degrees approaching the reciprocal relative thickness, or the reciprocal flattening, of the magnetized layer.

Analysis of observational spectra from Magsat by Cain et al. [1990] *on the reference sphere* indicates that the spectrum expected from random dipoles on a shell offers more satisfactory performance than a plain exponential spectrum. The former gives a lithospheric source depth for crustal fields instead of an ionospheric source altitude. This is also true when the reference spectrum is adjusted for a satellite altitude noise level. However, analysis of the noise adjusted observational spectrum *at satellite altitude* indicates that the random dipoles spectrum gives excessive source depths, while the plain exponential spectrum gives a broad range of leveling altitudes. The contrast suggests that the dominant part of the crustal magnetic spectrum is of an intermediate form which neither levels off, nor increases as rapidly as n^3 , on a lithospheric source shell. Such a form should be expected from correlated domain dipoles describing coherently magnetized geologic structures.



REFERENCES

- Backus, G., Poloidal and toroidal fields in geomagnetic field modeling, *Rev. Geophys.*, 24, 75-109, 1986.
- Cain, J.C., Z. Wang, C. Kluth, and D.R. Schmitz, Derivation of a geomagnetic field model to $n = 63$, *Geophys. J.*, 97, 431-441, 1989a.
- Cain, J.C., Z. Wang, D.R. Schmitz, and J. Meyer, The geomagnetic spectrum for 1980 and core-crustal separation, *Geophys. J.*, 97, 443-447, 1989b.
- Cain, J.C., B. Holter, and D. Sandee, Numerical experiments in geomagnetic modeling, *J. Geomag. Geoelectr.*, 42, 973-987, 1990.
- Jackson, A., Accounting for crustal magnetization in models of the core magnetic field, *Geophys. J. Int.*, 103, 657-673, 1990.
- Jackson, A., Statistical treatment of crustal magnetization, *Geophys. J. Int.*, 119, 991-998, 1994.
- Jackson, J.D., *Classical Electrodynamics*, John Wiley & Sons, New York, 1975.
- Langel, R.A., The Main Field, in *Geomagnetism*, Vol. 1, J. A. Jacobs, ed., Academic Press, 627 pp, 1987.
- Langel, R.A., and R.H. Estes, A geomagnetic field spectrum, *Geophys. Res. Lett.*, 9, 250-253, 1982.
- Lowes, F.J., Mean square values on the sphere of spherical harmonic vector fields, *J. Geophys. Res.*, 71, 2179, 1966.
- Lowes, F.J., Spatial power spectrum of the main geomagnetic field and extrapolation to the core, *Geophys. J. R. astr. Soc.*, 36, 717-730, 1974.
- McLeod, M.G., Statistical theory of the geomagnetic field and its secular variation, abstract in *Trans. Am. Geophys. Un.*, 66, 878, 1985.
- McLeod, M.G., Spatial and temporal power spectra of the geomagnetic field, submitted to *J. Geophys. Res.*, 1994.
- McLeod, M.G., Spatial and temporal power spectra of the geomagnetic field, *J. Geophys. Res.*, 101, 2745-2763, 1996.
- McLeod, M.G., and P.J. Coleman Jr., Spatial power spectra of the crustal geomagnetic field and the core geomagnetic field, *Phys. Earth Planet. Int.*, 23, 5-19, 1980.
- Nerem, R.S., F.J. Lerch, J.A. Marshall, E.C. Pavlis, B.H. Putney, B.D. Tapley, R.J. Eanes, J.C. Ries, B.E. Schultz, M.M. Watkins, S.M. Klosko, J.C. Chan, S.B. Luthcke, G.B. Patel, N.K. Pavlis, R.G. Williamson, R.H. Rapp, R. Biancale, and F. Nouel, Gravity Model Development for TOPEX/POSEIDON: Joint Gravity Models 1 and 2, *J. Geophys. Res.*, 99, 24,421-24,447, 1994.
- Ravat, D., R.A. Langel, M. Purucker, J. Arkani-Hamed, and D.E. Alsdorf, Global vector and scalar Magsat magnetic anomaly maps, *J. Geophys. Res.*, 100, 21,111-21,136, 1995.
- Sabaka, T.J., R.A. Langel, R.T. Baldwin, and J.A. Conrad, The geomagnetic field 1900-1995, including the large scale field from magnetospheric sources, and the NASA candidate models for the 1995 revision of the IGRF, *J. Geomag. Geoelectr.*, 49, 157-206, 1997.
- Voorhies, C.V., Magnetic location of Earth's core-mantle boundary and estimates of the adjacent fluid motion, Ph.D. thesis, Univ. of Colorado, 348 pp, 1984.
- Voorhies, C.V., and J. Conrad, Accurate predictions of mean geomagnetic dipole excursion and reversal frequencies, mean paleomagnetic field intensity, and the radius of Earth's core using McLeod's rule, NASA Technical Memorandum 104634, 35pp, 1996.



APPENDIX A

At the top of the viscous sub-layer, regarded as the sphere of radius c , the well-known magnetic induction equation,

$$\partial_t \mathbf{B} = \nabla \times (\mathbf{v} \times \mathbf{B}) + (\mu\sigma)^{-1} \nabla^2 \mathbf{B}, \quad (\text{A1})$$

reduces to the diffusion equation because of the no-slip boundary condition on the fluid velocity $\mathbf{v}(c, \theta, \phi; t) = \mathbf{0}$. Here μ and σ respectively denote core magnetic permeability and core electrical conductivity at the top of the sub-layer. The diffusion equation for the radial component of the core field is

$$\partial_t B_r = (\mu\sigma c)^{-1} \nabla^2 r B_r = (\mu\sigma)^{-1} / \partial_r^2 B_r, \quad (\text{A2})$$

where $/\partial_r^2 B_r /$ denotes the jump in the second radial derivative of B_r across the core-mantle interface. This jump in the curvature of the field lines is due to the jump in lateral electric current density across the boundary between the conducting core and the resistive mantle. Following Voorhies & Conrad [1996], the spherical harmonic expansion of (A1) is summarized via its coefficients

$$\partial_t g_{nc}^m [(n+1)(a/c)^{n+2}] \equiv (\mu\sigma)^{-1} J_n^m \quad (\text{A3})$$

$$\equiv (\mu\sigma)^{-1} (\pi k_{tm}^m)^2 g_{nc}^m [(n+1)(a/c)^{n+2}]. \quad (\text{A4})$$

Equation (A3) defines the current density jump coefficient J_n^m ; (A4) defines an effective modal scale height $[k_{tm}^m(t)]^{-1}$ which may be either real or imaginary. Similar relations can be written for $\partial_t h_{nc}^m$ in terms of J_n^m and $k_{tm}^m(t)$.

Summing the squares of these relations over orders m and dividing by $(n+1)$ yields

$$F_{nc}(c) = (\pi^2/\mu\sigma)^2 (n+1)(a/c)^{2n+4} \sum_{m=0}^n [(k_{tm}^m)^4 (g_{nc}^m)^2 + (k_{tm}^m)^4 (h_{nc}^m)^2] \quad (\text{A5})$$

$$\equiv (\mu\sigma)^{-2} (\pi k_{tm}^m)^4 R_{nc}(c) \quad (\text{A6})$$

which defines positive k_{tm}^m . $[k_{tm}^m]^{-1}$ is the effective scale height for harmonic degree n . Upward continuation of (A5) to any radius $r \geq c$ gives

$$F_{nc} = (\mu\sigma)^{-2} (\pi k_{tm}^m)^4 R_{nc}. \quad (\text{A7})$$

The expectation value of (A7) yields (4c), with the understanding that the contribution to $\{F_n\}$ from $\{\pi k_{tm}^m\}^4 \{R_n\} \approx (\pi k_{tm}^m)^4 \{R_n\}$ is of more immediate concern than are correlated fluctuations in $(k_{tm}^m)^4$ and R_n .

APPENDIX B

The integral in the ellipticity correction (35) is

$$Q_n = \int_0^1 (1 + \gamma^2 x^2)^{-n-1} [1 + \alpha^2 x^2]^{1/2} dx \quad (\text{B1a})$$

where

$$\alpha^2 \equiv (\gamma^2 + \varepsilon^2)/(1 - \varepsilon^2) = \gamma^2(2 - \varepsilon^2)/(1 - \varepsilon^2)$$

$$= 2\gamma^2 + \gamma^4. \quad (\text{B1b})$$

Because $\gamma^2 \ll 1$, we approximate $(1 + \alpha^2 x^2)^{1/2} \approx 1 + \gamma^2 x^2$ and

$$Q_n = \int_0^1 (1 + \gamma^2 x^2)^{-n} dx \equiv Z_n / \gamma. \quad (\text{B2})$$

The integrand is expanded in powers of $(\gamma x)^2 \ll 1$

$$Z_n = \gamma \int_0^1 \sum_{j=0}^{\infty} \frac{(n+j-1)!}{(n-1)!j!} (-\gamma^2)^j x^{2j} dx, \quad (\text{B3})$$

integrated term by term, and evaluated at the limits

$$Z_n = \sum_{j=0}^n \frac{(n+j-1)!}{(n-1)!j!} \frac{(-\gamma^{2j+1})}{(2j+1)}. \quad (\text{B4})$$

Equation (B4) is rewritten as the sum of indefinite integrals

$$Z_n = \sum_{j=0}^n \frac{(n+j-1)!}{(n-1)!j!} \int (-\gamma)^{2j} d\gamma \quad (\text{B5})$$

which is equal to the indefinite integral of the sum

$$Z_n = \int \sum_{j=0}^n \frac{(n+j-1)!}{(n-1)!j!} (-\gamma^2)^j d\epsilon \quad (\text{B6})$$

$$= \int (1 + \gamma^2)^{-n} d\gamma. \quad (\text{B7})$$

To obtain the recursion relation for Z_n , note

$$\frac{d}{d\gamma} [\gamma(1 + \gamma^2)^{-n}] = (1 + \gamma^2)^{-n} - 2n\gamma^2(1 + \gamma^2)^{-n-1} \quad (\text{B8})$$

$$= -(2n-1)\gamma^2(1 + \gamma^2)^{-n-1} + (1 + \gamma^2)^{-n-1}; \quad (\text{B9})$$

therefore, integration of (B7) by parts and back substitution from (B9) yields

$$Z_n = \gamma(1 + \gamma^2)^{-n} + 2n \int \gamma^2 (1 + \gamma^2)^{-n-1} d\gamma \quad (\text{B10})$$

$$= [2n Z_{n+1} - \gamma(1 + \gamma^2)^{-n}] / (2n - 1). \quad (\text{B11})$$

Equations (B11) and (B2) give the recursion relations

$$Q_{n+1} \approx [(2n-1)Q_n + (1 + \gamma^2)^{-n}] / (2n). \quad (\text{B12})$$

Detailed calculations, initialized with $Q_1 \approx 1 - \gamma^2/3$, show that (B12) underestimates Q_n by about 4 parts per million. This is mainly due to omission of a factor of about $(1 + \gamma^4/12)$.

REPORT DOCUMENTATION PAGE

Form Approved
OMB No. 0704-0188

Public reporting burden for this collection of information is estimated to average 1 hour per response, including the time for reviewing instructions, searching existing data sources, gathering and maintaining the data needed, and completing and reviewing the collection of information. Send comments regarding this burden estimate or any other aspect of this collection of information, including suggestions for reducing this burden, to Washington Headquarters Services, Directorate for Information Operations and Reports, 1215 Jefferson Davis Highway, Suite 1204, Arlington, VA 22202-4302, and to the Office of Management and Budget, Paperwork Reduction Project (0704-0188), Washington, DC 20503.

1. AGENCY USE ONLY <i>(Leave blank)</i>		2. REPORT DATE December 1998	3. REPORT TYPE AND DATES COVERED Technical Publication	
4. TITLE AND SUBTITLE Elementary Theoretical Forms for the Spatial Power Spectrum of Earth's Crustal Magnetic Field			5. FUNDING NUMBERS	
6. AUTHOR(S) C. Voorhies				
7. PERFORMING ORGANIZATION NAME(S) AND ADDRESS (ES) Goddard Space Flight Center Greenbelt, Maryland 20771			8. PERFORMING ORGANIZATION REPORT NUMBER 99B00004	
9. SPONSORING / MONITORING AGENCY NAME(S) AND ADDRESS (ES) National Aeronautics and Space Administration Washington, DC 20546-0001			10. SPONSORING / MONITORING AGENCY REPORT NUMBER 1998—TP—208608	
11. SUPPLEMENTARY NOTES				
12a. DISTRIBUTION / AVAILABILITY STATEMENT Unclassified - Unlimited Subject Category:46 Report available from the NASA Center for AeroSpace Information, Parkway Center/7121 Standard Drive, Hanover, Maryland 21076-1320			12b. DISTRIBUTION CODE	
13. ABSTRACT <i>(Maximum 200 words)</i> The magnetic field produced by magnetization in Earth's crust and lithosphere can be distinguished from the field produced by electric currents in Earth's core because the spatial magnetic power spectrum of the crustal field differs from that of the core field. Theoretical forms for the spectrum of the crustal field are herein derived by treating each magnetic domain in the crust as the point source of a dipole field. The geologic null-hypothesis that such moments are uncorrelated is used to obtain the magnetic spectrum expected from a randomly magnetized, or unstructured, spherical crust of negligible thickness. This simplest spectral form is modified to allow for uniform crustal thickness, ellipsoidality, and the polarization of domains by an aperiodically reversing, geocentric axial dipole field from Earth's core. Such spectra are intended to describe the background crustal field. Magnetic anomalies due to correlated magnetization within coherent geologic structures may well be superimposed upon this background; yet representing each such anomaly with a single point dipole may lead to similar spectral forms. Results from attempts to fit these forms to observational spectra, determined via spherical harmonic analysis of MAGSAT data, are summarized in terms of amplitude, source depth, and misfit. Each theoretical spectrum reduces to a source factor multiplied by the usual exponential function of spherical harmonic degree n due to geometric attenuation with altitude above the source layer. The source factors always vary with n and are approximately proportional to n^3 for degrees 12 through 120. The theoretical spectra are therefore not directly proportional to an exponential function of spherical harmonic degree n . There is no radius at which these spectra are flat, level, or otherwise independent of n .				
14. SUBJECT TERMS Geosciences, Geophysics, Geomagnetism, Crustal Field, Magnetic Spectrum			15. NUMBER OF PAGES 36	
			16. PRICE CODE	
17. SECURITY CLASSIFICATION OF REPORT Unclassified	18. SECURITY CLASSIFICATION OF THIS PAGE Unclassified	19. SECURITY CLASSIFICATION OF ABSTRACT Unclassified	20. LIMITATION OF ABSTRACT UL	

